

Rocket dust storms and detached layers in the Martian atmosphere

Aymeric Spiga^{*1}, Julien Faure¹, Jean-Baptiste Madeleine^{1,3}, Anni Määttänen², and François Forget¹

¹Laboratoire de Météorologie Dynamique (LMD), Université Pierre et Marie Curie (UPMC), Institut Pierre Simon Laplace (IPSL), Centre National de la Recherche Scientifique (CNRS), Paris, France

²Laboratoire ATmosphère, Milieux et Observations Spatiales (LATMOS), CNRS, Guyancourt, France

³Brown University, Providence, Rhode Island, USA

Airborne dust is the main climatic agent in the Martian environment. Local dust storms play a key role in the dust cycle; yet their life cycle is poorly known. Here we use mesoscale modeling with radiatively-active transported dust to predict the evolution of a local dust storm monitored by OMEGA on board Mars Express. We show that the evolution of this dust storm is governed by deep convective motions. The supply of convective energy is provided by the absorption of incoming sunlight by dust particles, in lieu of latent heating in moist convection on Earth. We propose to use the terminology “rocket dust storm”, or conio-cumulonimbus, to describe those storms in which rapid and efficient vertical transport takes place, injecting dust particles at high altitudes in the Martian troposphere (30 to 50 km). Combined to horizontal transport by large-scale winds, rocket dust storms form detached layers of dust reminiscent of those observed with instruments on board Mars Global Surveyor and Mars Reconnaissance Orbiter. Detached layers are stable over several days owing to nighttime sedimentation being unable to counteract daytime convective transport, and to the resupply of convective energy at sunrise. The peak activity of rocket dust storms is expected in low-latitude regions at clear season, which accounts for the high-altitude tropical dust maximum unveiled by Mars Climate Sounder. Our findings on dust-driven deep convection have strong implications

for the Martian dust cycle, thermal structure, atmospheric dynamics, cloud microphysics, chemistry, and robotic and human exploration.

1 Introduction

The Martian atmosphere has a permanent thin veil of suspended dust particles, the amount varying with location and season. The dust cycle is a crucial component of the Martian climatic system and the main factor of interannual variability (Smith, 2004; Montabone et al., 2005). Airborne dust scatters and absorbs incoming sunlight and, to a lesser extent, outgoing thermal radiation (Gierasch and Goody, 1972). This results in a significant warming of the Martian atmosphere, even in moderately dusty conditions. It is thus of key interest to characterize the spatial and temporal variability of dust in the Martian atmosphere and the control through lifting from the surface, transport by atmospheric winds and sedimentation.

The Martian tropospheric circulation is active at all spatial scales. This yields a variety of structures formed by dust lifted and transported by atmospheric winds (Cantor et al., 2001; Spiga and Lewis, 2010, Figure 1), which in turn change the Martian surface albedo (Szwast et al., 2006). Large-scale circulations, such as Hadley cells and baroclinic waves, induce dust transport over interhemispheric distances (Wang et al., 2003). Mesoscale circulations, which

^{*}Corresponding author: aymeric.spiga@upmc.fr

typical scales range from a few 100s kilometers to a few kilometers, give rise to dusty fronts along polar cap edges (Toigo et al., 2002), dust transport through slope winds (Rafkin et al., 2002) and local or regional dust storms (Malin et al., 2008; Rafkin, 2009; Määttä et al., 2009). Turbulent eddies in the Planetary Boundary Layer [PBL] cause gusts and vortices a few tens of meters wide, which can lift and transport dust, forming the frequently observed “dust devils” (Thomas and Gierasch, 1985; Balme and Greeley, 2006). In addition to those phenomena encountered in the Martian atmosphere every year, a thick global dust loading occurs near perihelion with irregular interannual variability (Zurek and Martin, 1993; Montabone et al., 2005; Cantor, 2007). This phenomenon is often referred to as a “global dust storm”, despite the global dust cover not being related to an unique global storm but to the combined action of interhemispheric transport and regional dust storms growing unusually large.

The Martian dust cycle is characterized by strong radiative-dynamical feedbacks. On the one hand, the amount of dust in the atmosphere is closely related to atmospheric circulations through lifting and transport. On the other hand, airborne dust impacts thermal structure, hence atmospheric circulations at all scales. Thus far, the interplay between dynamical and radiative phenomena controlling the dust cycle have been mostly studied with Global Climate Models (GCMs) (Haberle et al., 1982; Leovy, 1985). Dust-lifting parameterizations were included in GCMs to better explore those radiative-dynamical feedbacks (Murphy et al., 1995; Newman et al., 2002; Basu et al., 2006; Kahre et al., 2006). As pointed out by Rafkin (2009), the GCM approach suffers two main limitations. Firstly, GCM results are very sensitive to the choice of free parameters in the dust lifting and dust devil parameterizations. Secondly, lifting and transport phenomena within local, regional and global dust storms are associated with mesoscale circulations left unresolved by GCMs. Rafkin (2009) demonstrated through idealized three-dimensional simulations how mesoscale modeling permits to investigate the initiation and amplification of Martian dust storms through radiative-dynamical feedbacks in greater details and physical consistency

than GCMs.

The interest for dynamical processes controlling the spatial distribution of dust in the Martian atmosphere has been renewed by recent observations which completed pioneering observations on board Mariner and Viking (Anderson and Leovy, 1978; Jaquin et al., 1986). Using Mars Express stellar occultations, Montmessin et al. (2006) confirmed the occurrence of high-altitude detached hazes discovered in Mariner and Viking data, although the nature of aerosols (dust or ice) remained ambiguous. Mars Climate Sounder [MCS] observations by McCleese et al. (2010) and Heavens et al. (2011a) demonstrated that the vertical distribution of dust exhibits “detached layers” in apparent contradiction with the equilibrium between large-scale mixing and sedimentation assumed thus far (Conrath, 1975). Heavens et al. (2011b) listed several possible scenarios (described in section 5.2) to account for those phenomena. In most cases, mesoscale and turbulent circulations appear to play a key role. Through Mars Global Surveyor [MGS] Thermal Emission Spectrometer [TES] measurements during the 2001 global dust storm, Clancy et al. (2010) also concluded that the observed dust vertical distribution implies “extraordinary vertical advection velocities”.

In this context, further studies of dusty mesoscale circulations and their radiative-dynamical feedbacks are needed to broaden the knowledge of the Martian dust cycle and, more generally, of the Martian climate and meteorology. What is the evolution and fate of local dust storms on Mars? How do temperature and winds in the Martian atmosphere respond to such disturbances? What is their influence on the distribution of dust particles? How could we characterize the mesoscale variability left unresolved by GCMs? Our original approach to address those key questions consists in modeling the evolution of a typical mesoscale storm observed in unprecedented detail by orbital infrared spectrometry (Määttä et al., 2009). A summary of this observation is proposed in section 2. Our modeling strategy to simulate the storm is based on an upgraded version of the mesoscale model by Spiga and Forget (2009), detailed in section 3. The predicted evolution of the mesoscale dust storm and its impact on the dust distribution are analyzed in sec-

tion 4. We discuss the implications and perspectives of our findings in section 5.

2 The OMEGA dust storm

In a northern summer afternoon of Martian Year 27 ($L_s = 135^\circ$, local time 1330), the OMEGA instrument on board Mars Express observed strong evidence of a local, optically very thick dust storm centered at $(25^\circ\text{E}, 2.5^\circ\text{S})$. Hereinafter we refer to this event as the “OMEGA storm”. The OMEGA storm took place in a region and at a season characterized by low dust storm activity (Cantor et al., 2001, 2006, Figure 17). Määttänen et al. (2009) used the OMEGA measurements to map optical thickness inside the storm (Figure 1) and to retrieve optical properties of the Martian dust. An observation acquired 3 sols earlier at the same location showed an essentially clear atmosphere, devoid of thick dust disturbances. The rapid onset and development of the OMEGA dust storm, peaking at visible optical thickness of 10 in only three sols, are remarkable. Interestingly, using the same OMEGA observation three sols before the storm, Spiga et al. (2007) found strong perturbations in the surface pressure field retrieved from the $2\ \mu\text{m}$ CO_2 line, suggesting that strong winds were already present and interacting with topography.

Analysis of Figure 1 shows significant variability in optical depth within the OMEGA storm which exhibits a complex, convective-looking, mesoscale structure. Simultaneous Planetary Fourier Spectrometer [PFS] measurements of temperature structure also revealed how the Martian atmospheric state is impacted by this dust disturbance (Määttänen et al., 2009). Preliminary assessment of dust vertical distribution through single-column atmospheric modeling pointed towards low-altitude confinement of dust in the storm; yet these conclusions could not be fully reconciled with OMEGA nadir measurements. All these elements advocate for dedicated three-dimensional mesoscale modeling of the OMEGA storm. Moreover, further storm development and decay could not be followed by OMEGA in lack of Mars Express nadir data at the following ground track overlap three sols later. Thus, only a

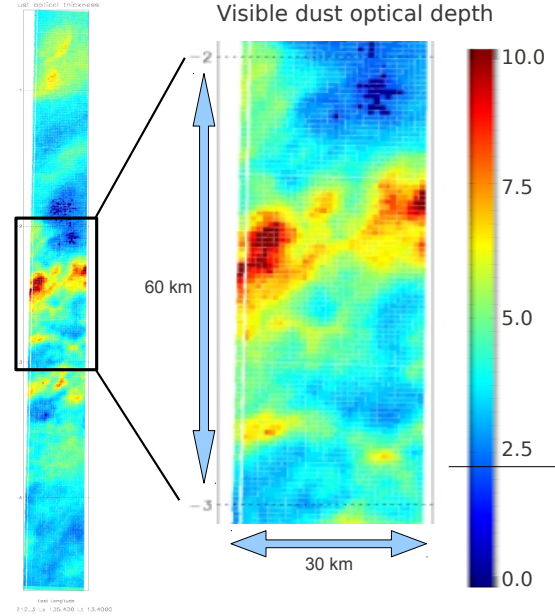


Figure 1: Column dust optical depth at $1\ \mu\text{m}$ observed by OMEGA in Terra Meridiani. The zoomed area is located at coordinates $(25^\circ\text{E}, 2.5^\circ\text{S})$. Values below the horizontal line in the colorbar cannot be considered as reliable. Adapted from Määttänen et al. (2009) with permission.

detailed modeling study could help to reveal the evolution of the OMEGA storm.

To complement OMEGA observations in Määttänen et al. (2009), we sought for MGS Mars Orbiting Camera [MOC] images (Wang and Ingersoll, 2002). Only global image mosaics acquired at local time 1400 could be used to attempt a tracking of the development and dissipation of the OMEGA storm. MOC images obtained for sols around the OMEGA storm are assembled in Figure 2. At $L_s = 132^\circ$ the Martian atmosphere is clear in the region where the OMEGA storm occurred (marked with a red circle). At $L_s = 135^\circ$, close to the time of OMEGA measurements, the storm appears in the MOC image (unfortunately, MOC

images one sol before had a gap in observations exactly at the storm location). At $L_s = 136 - 137^\circ$, dust storm activity in the region continues during several sols and exhibits strong sol-to-sol variations and horizontal transport. This activity might be the result of either several individual short-lived (less than a sol) storms occurring in the same region, or one storm that was particularly variable both temporally and spatially.

3 Modeling methodology

3.1 Mesoscale model and general settings

To study the evolution of the OMEGA dust storm, we employ the “Laboratoire de Météorologie Dynamique” (LMD) Martian Mesoscale Model (MMM) (Spiga and Forget, 2009; Spiga et al., 2011). This mesoscale model is built by coupling a three-dimensional, fully compressible, non-hydrostatic dynamical core, capable to resolve fine-scale circulations on Earth (Skamarock and Klemp, 2008), with the complete set of Martian physical parameterizations used in the LMD-GCM (Forget et al., 1999; Madeleine et al., 2011). The LMD-MMM has the capability to advect an arbitrary number of tracers. Initial and boundary conditions for the LMD-MMM are provided by LMD-GCM simulations which use similar physical parameterizations, thereby reducing inconsistencies.

Details about the LMD-MMM and typical test simulations can be found in Spiga and Forget (2009). Physical parameterizations described in this reference paper have been recently improved. The multi-size dust radiative transfer introduced by Madeleine et al. (2011) is now employed in both the LMD-GCM and the LMD-MMM. Dust optical properties (extinction function, single-scattering albedo and asymmetry factor) are computed using the most recent optical indices retrieved by Wolff et al. (2009). The advected tracers describing the distribution of dust aerosols are radiatively active, allowing for detailed analysis of the dust radiative-dynamical feedbacks. Additional details about this interactive dust scheme

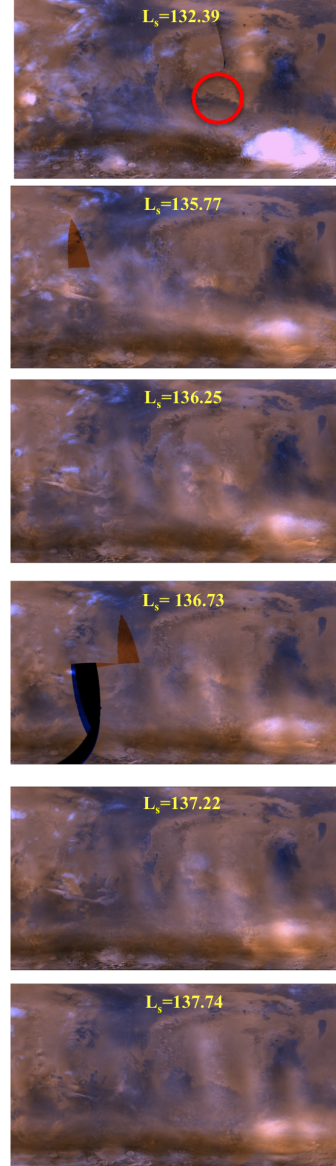


Figure 2: Mars Daily Global Map retrieved with MOC instrument on board MGS. Images obtained with the “Mars Climate Center” website hosted by Ashima Research.

and the initialization of the OMEGA storm are provided in sections 3.2 and 3.3. Multisize particle sedimentation is computed using Stokes' law and Cunningham correction factors (Rossow, 1978). The shape of dust particles is accounted for by an additional factor β in the second term of the Cunningham correction factor. We adopt $\beta = 0.5$ (disk-shaped dust particles) in the LMD-MMM as is done in the LMD-GCM (Madeleine et al., 2011). The evolution of the OMEGA storm predicted by the model is not sensitive to this parameter: similar results are obtained with $\beta = 1$ (spherical dust particles).

The mesoscale domain employed for dust storm simulations is centered in Terra Meridiani at the approximate location of the OMEGA storm ($25^\circ\text{E}, 2.5^\circ\text{S}$). It comprises 181×181 horizontal grid points with 7 km grid spacing (simulations with 10 km grid spacing were also performed and yield similar results). Figure 3 shows the location and extent of the mesoscale domain projected on the Martian globe. Along the vertical dimension, 101 levels are set with a spacing less than 1 km for altitudes below 40 km (Figure 3). LMD-MMM integrations are carried out with a timestep of 20 s, except for radiative transfer computations which are performed every 120 s (about 1/31st of a Martian hour). This allows for radiative-dynamical feedbacks to be taken into account: changes in dust distribution rapidly impact the thermal structure. Mesoscale simulations are started at local time 1330 and carried out in late northern summer ($L_s = 135^\circ$) when the OMEGA storm was monitored. Whenever different starting local time or L_s are considered (section 4.2 and 5.1), initial and boundary conditions provided to the LMD-MMM by the LMD-GCM are recomputed.

3.2 Interactive dust scheme and related diagnostics

The radiative impact at wavelength λ of the total quantity of dust in the atmospheric column is given by the column optical depth τ_λ

$$\tau_\lambda = \int_{\text{column}} d\tau_\lambda \quad (1)$$

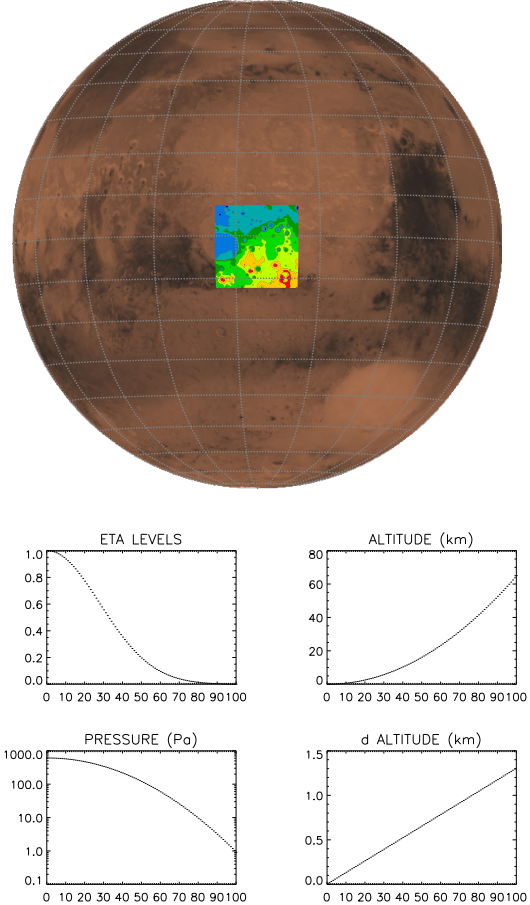


Figure 3: LMD-MMM settings for dust storm simulations. Top plot shows horizontal domain which comprises 181×181 horizontal grid points with 7 km grid spacing. Bottom plot shows vertical discretization which comprises 101 levels. Pressure at the top of the mesoscale domain is 1 Pa. x -axis denotes model vertical levels. y -axis corresponds to (top left panel) mass-based coordinate, cf. Spiga and Forget (2009), (top right panel) altitude, (bottom left panel) pressure and (bottom right panel) distance between vertical levels. Values for altitude and pressure are computed with standard surface pressure 610 Pa and scale height 10 km; the actual model top in simulations is at ~ 55 km altitude.

The contribution $d\tau_\lambda$ to the column optical depth of a layer of dust of elementary thickness dP , where P is atmospheric pressure, writes

$$d\tau_\lambda = \xi \frac{Q_{\text{ext},\lambda}}{r_{\text{eff}}} q dP \quad \text{with} \quad \xi = \frac{3}{4\rho_{\text{dust}} g} \quad (2)$$

where ρ_{dust} is the dust particle density (about 2500 kg m^{-3}), g the acceleration of gravity, q the mass mixing ratio, r_{eff} the effective radius, and $Q_{\text{ext},\lambda}$ the dust extinction efficiency which is a function of r_{eff} . For the sake of comparison with existing diagnostics in the literature, e.g. MCS retrievals (Heavens et al., 2011a), the density-scaled optical depth $\delta_z \tau_\lambda$ may be employed instead of $d\tau_\lambda$

$$\delta_z \tau_\lambda = \frac{-1}{\rho} \frac{d\tau_\lambda}{dz} = \frac{g}{dP} d\tau_\lambda = g \xi \frac{Q_{\text{ext},\lambda}}{r_{\text{eff}}} q \quad (3)$$

where ρ is atmospheric density. In what follows, λ subscripts are dropped for conciseness. Except otherwise indicated, dust optical depths are expressed at $\lambda = 0.67 \text{ } \mu\text{m}$. The conversion of dust optical depths and radiative properties from this wavelength to others, and vice-versa, is detailed in Madeleine et al. (2011). To compare quantities expressed at $0.67 \text{ } \mu\text{m}$ with MCS observations in the A5 channel at $21.6 \text{ } \mu\text{m}$, we rely on the approximation

$$\frac{\delta_z \tau}{\delta_z \tau_{\text{mcs}}} \simeq 7.3 \quad (4)$$

as advised by Heavens et al. (2011a) (this is consistent with Figure 1 in Madeleine et al., 2011).

In LMD-MMM simulations, it is assumed that the sizes of the dust particles in any atmospheric layer follow a lognormal distribution of constant standard deviation σ_0 (Madeleine et al., 2011). Under this assumption, the particle size distribution is fully described by the mass mixing ratio q and the dust number density N (this method is often referred to as a “two-moment” scheme). The effective radius r_{eff} is then proportional to the cube root of q/N

$$r_{\text{eff}} = \mathcal{A} \sqrt[3]{\frac{q}{N}} \quad \text{with} \quad \mathcal{A} = \sqrt[3]{\frac{g\xi}{\pi}} e^{\sigma_0^2} \quad (5)$$

Thus the dust distribution in the LMD-MMM is merely predicted using two tracers $[q, N]$. Those

fields are modified at each model iteration by advection (i.e. transport by winds), sources (lifting) and sinks (sedimentation). The radiative impact of the resulting dust distribution $[q, N]$ is accounted for using equations 2 and 5. Through this interactive dust scheme, our mesoscale model offers a physically-consistent extrapolation of the storm structure and behavior from the instantaneous observation by OMEGA. In what follows, the evolution of the simulated dust storm is diagnosed by the dust optical depth quantities τ and $\delta_z \tau$ computed using equations 1 to 5 and predicted fields $[q, N]$ in the LMD-MMM.

3.3 Setting up the dust storm disturbance

LMD-MMM storm simulations are based on initial and boundary conditions obtained from LMD-GCM simulations. The interactive dust scheme described in section 3.2 is used in both models. Column dust optical depths τ_{TES} measured by TES for a typical year devoid of global dust storms are employed to constrain $[q, N]$ in the LMD-GCM, so that column optical depths τ_{back} in this model verify

$$\tau_{\text{back}} = \xi \int_{\text{column}} \frac{Q_{\text{ext}}}{r_{\text{eff}}} q dP = \tau_{\text{TES}} \quad (6)$$

This dust distribution is thought to be representative of large-scale “background” dustiness. Initial background fields in the LMD-MMM are denoted $[q_0, N_0]$ and $\tau_{\text{back},0}$.

To define an initial storm perturbation in the LMD-MMM, a local dust perturbation δq is added to the initial background mass mixing ratio q_0 . The dust perturbation δq is designed to mimic the column optical depth τ_{storm} of the mesoscale storm monitored by the OMEGA mapping spectrometer at $1 \text{ } \mu\text{m}$ (Figure 1). It is defined such that

$$\tau_{\text{storm}} = \xi \int_{\text{column}} \frac{Q_{\text{ext}}}{r_{\text{eff}}} (q_0 + \delta q) dP \quad (7)$$

The initial dust perturbation δq is assumed to extend down to the surface where pressure is P_{surf} . We define P_{top} as the pressure at the top of the dust

perturbation. Above the dust storm, for pressures P such that $P < P_{\text{top}}$, we set $\delta q = 0$. Within the dust storm, for pressures P such that $P_{\text{top}} < P < P_{\text{surf}}$, we assume for simplicity that δq is constant with pressure P , which yields

$$\delta q = (\tau_{\text{storm}} - \tau_{\text{back},0}) \left[\xi \int_{P_{\text{top}}}^{P_{\text{surf}}} \frac{Q_{\text{ext}}}{r_{\text{eff}}} dP \right]^{-1} \quad (8)$$

The vertical distribution of dust within the OMEGA storm is not known. The rationale for choosing δq constant with height within the storm is simplicity and the fact that afternoon PBL convection yields well-mixed dust within a few hundreds of seconds (e.g. Spiga et al., 2010). Results are not critically sensitive to this initial assumption. Conversely, the evolution of the OMEGA storm is sensitive to the pressure P_{top} at the top of the dust perturbation, which is not constrained by OMEGA observations either. The impact of the vertical extent of the storm disturbance is thus left to be explored in the modeling analysis (section 4.2.2).

In the horizontal dimension, the storm area is a disk of center (25°E, 2.5°S) and radius R_{storm} where the dust perturbation δq is uniform. Outside the storm area, we set $\delta q = 0$. To avoid sharp discontinuities at the storm boundaries, a transition zone of a few horizontal grid points is prescribed with hyperbolic tangent functions between inside and outside the storm.

Once the perturbed mixing ratio $q'_0 = q_0 + \delta q$ is computed using equations 6 and 8, the number density N'_0 follows from equation 5. We assume that the initial dust effective radius r_{eff} is left unaffected by adding the storm perturbation upon background conditions. In the season and location considered for our mesoscale simulations, this yields $r_{\text{eff}} \simeq 1.5$ microns, which is also the value assumed by Määttä et al. (2009) for OMEGA retrievals. However, larger dust effective radius r_{eff} are often observed in dust storms (Clancy et al., 2010; Elteto and Toon, 2010). Hence we also carry out simulations where r_{eff} is set to $3 \mu\text{m}$ within the storm perturbation (see section 4.2.2). In this case, dust optical properties, notably Q_{ext} , are recomputed before equation 8 is used to obtain q'_0 .

4 Results

4.1 Reference simulation

The reference case study for the evolution of the OMEGA storm is defined as follows. The adopted dust optical depth in the storm perturbation is $\tau_{\text{storm}} = 4.25$ over an area of radius $R_{\text{storm}} = 0.5^\circ$ ($\simeq 30$ km). The value $\tau_{\text{storm}} \simeq 4$ does not account for local maxima within the storm reaching 10, but reflects instead the averaged storm conditions monitored on board Mars Express by OMEGA (Figure 1) and PFS (see Määttä et al., 2009). We choose P_{top} so that the initial dust storm perturbation is 10 km high, which corresponds to dust particles being mixed within the convective PBL and the lowermost layers of the free troposphere. In the reference simulation, dust lifting is not included: only the evolution of the storm perturbation witnessed by OMEGA is considered. The sensitivity of model predictions to those various settings is discussed in section 4.2.

Figure 4 (left) shows the predicted column dust optical depth τ every two hours from local time 1400 to 0000. By the end of the afternoon, the dust storm appears to have drifted in the southwest direction, while its column optical depth τ has been divided by a factor of two. What OMEGA saw as an optically thick dust storm in early afternoon becomes, according to LMD-MMM simulations, a dust disturbance hardly discernible from background dust conditions in the middle of the night. In other words, our mesoscale simulations predict a rapid decay and short lifetime for the OMEGA dust storm. This tends to indicate that the spatial variability observed in MOC images in Figure 2 would correspond to several short-lived dust storms rather than a single, highly variable, dust storm event.

The “nadir view” of the OMEGA dust storm in Figure 4 (left) does not reveal the most notable characteristics of its evolution. Figure 4 (right) shows the corresponding “limb view” through longitude-altitude sections of “MCS-like” density-scaled dust optical depth $\delta_z \tau_{\text{mcs}}$ at $21.6 \mu\text{m}$ (cf. also movie in supplementary material). Within few hours, the dust storm disturbance evolves into a dusty plume

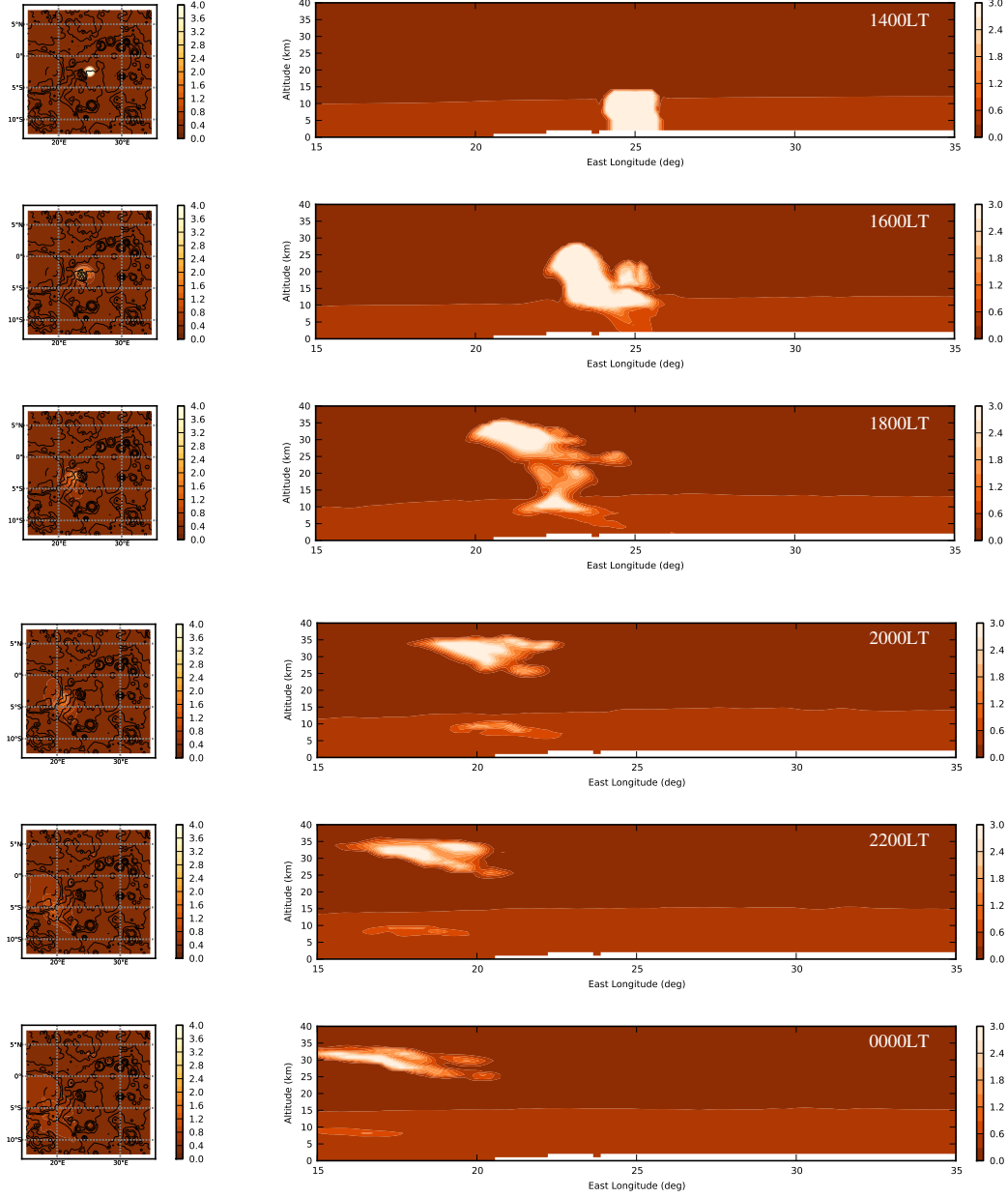


Figure 4: LMD-MMM reference simulation of the OMEGA storm. (left) Latitude-longitude maps of column dust optical depth τ at $0.67 \mu\text{m}$ and (right) longitude-altitude sections of “MCS-like” density-scaled dust optical depth $\delta_z \tau_{\text{MCS}}$ at $21.6 \mu\text{m}$ in $10^{-3} \text{ m}^2 \text{ kg}^{-1}$. Sections are obtained at latitude 2.5°S . Season is late northern summer ($L_s = 135^\circ$). Diagnostics are shown every two hours from local time 1400 to 0000.

rising from lower to upper troposphere. The dusty plume reaches altitudes as high as 30–35 km around sunset. Then dust particles undergo significant horizontal transport and the storm loses its vertical extent to appear as a high-altitude elongated dust cloud. To summarize, mesoscale modeling predicts that within 6 hours the low-level dust disturbance monitored by OMEGA would turn into a fast-rising dust plume then a clear-cut high-altitude detached layer of dust. According to our model predictions, the implied horizontal and vertical advection of dust is spectacular: the vast majority of dust particles within the initial storm perturbation are transported well above the PBL to the higher troposphere and over horizontal distances reaching nearly a thousand kilometers (dust particles are even transported out of the mesoscale domain). This daytime dynamical transport accounts for the brief lifetime of the storm; sedimentation does not appear as a key factor.

The plume-like appearance of the dust storm in Figure 4 denotes deep convective motions. This is confirmed by analyzing vertical winds predicted by the LMD-MMM. Figure 5 shows that updrafts within the dust storm often reach amplitudes $> 3 \text{ m s}^{-1}$, peaking as high as $8 - 10 \text{ m s}^{-1}$, while compensating subsidences reach $1 - 2 \text{ m s}^{-1}$. These values are about two orders of magnitude larger than typical vertical advection velocities obtained through GCM simulations ($\sim 10^{-1} \text{ m s}^{-1}$). Our predictions for vertical velocities in dust storms are in line with mesoscale simulations of Rafkin (2009) (Figure 11) and Rafkin (2012) (Figure 3), as well as discussions in Clancy et al. (2010) and Heavens et al. (2011b) about powerful transport processes possibly accounting for the observed vertical distribution of dust on Mars. The predicted vertical wind field in Figure 5 also features, above the storm central updraft, alternating patterns reminiscent of upward-propagating gravity waves.

Local dust storms such as the OMEGA storm have been sometimes referred to as “dust bombs”; we propose instead the terminology “rocket dust storms” to better emphasize how rapid and powerful the vertical transport can be. Alternatively those phenomena can be named conio-cumulonimbus, using *konios* the Greek word for dust (Heavens et al., 2011b). This emphasizes the analogy with pyro-cumulonimbus on

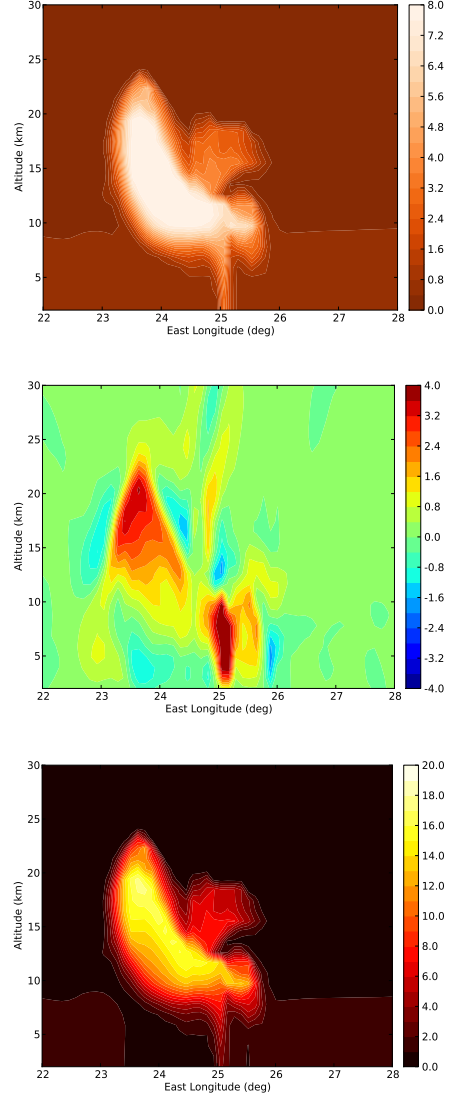


Figure 5: LMD-MMM reference simulation of the OMEGA storm. Longitude-altitude sections obtained at local time 1500 and latitude 2.5°S . From top to bottom: (a) MCS-like density-scaled optical depth at $21.6 \mu\text{m}$ in $10^{-3} \text{ m}^2 \text{ kg}^{-1}$; (b) Vertical wind in m s^{-1} (maximum is about 10 m s^{-1}); (c) Short-wave heating rate in K per Martian hour (maximum is about 24 K/h).

Earth, associated with wildfires and thought to be responsible for detached layers of aerosols in the terrestrial stratosphere (Fromm et al., 2010).

Absorption of incoming sunlight by transported dust is the driving mechanism for the deep convective motions in rocket dust storms, playing the role devoted to latent heat in terrestrial moist convective storms. Radiative heating rates \mathcal{H}_{SW} in shortwave (visible) wavelengths are displayed in Figure 5. Shortwave absorption by dust particles transported within the storm yields an extreme warming of 15 – 20 K per Martian hour in atmospheric layers where density-scaled optical depth is large. Below those layers, and at the surface, extinction yields moderate shortwave radiative warming, which does not appear to lead to significant dynamical effects. Absorption by dust particles in infrared wavelengths also warms the atmosphere though one order of magnitude less than shortwave absorption. Radiative warming within the dust storm disturbance causes the atmosphere to become positively buoyant, which gives rise to strong upward convective motions.

Figure 6 shows through a latitude-altitude section how rocket dust storms impact thermal structure. Compared to background temperature conditions, atmosphere is warmer above/within the maximum in density-scaled optical depth and cooler below it. This appears in qualitative agreement with PFS temperature measurements over the OMEGA storm (Figure 8 in Määttä et al., 2009) which features a positive temperature anomaly in the troposphere and a negative one near the surface. This probably means that the OMEGA storm has already started its ascent at the initial local time considered in reference simulation (this scenario is explored in section 4.2.2 and does not change the results presented here).

The impact of rocket dust storm on temperature structure is best accounted for by analyzing potential temperature in Figure 6. From the Lagrangian point of view (following an ascending dusty parcel), potential temperature θ is only modified through diabatic processes \mathcal{J}

$$\frac{D\theta}{Dt} = \mathcal{J} \quad \text{with} \quad \theta = T \mathcal{P}^{-1} \quad \text{and} \quad \mathcal{J} = \frac{\mathcal{H}}{c_p} \mathcal{P}^{-1} \quad (9)$$

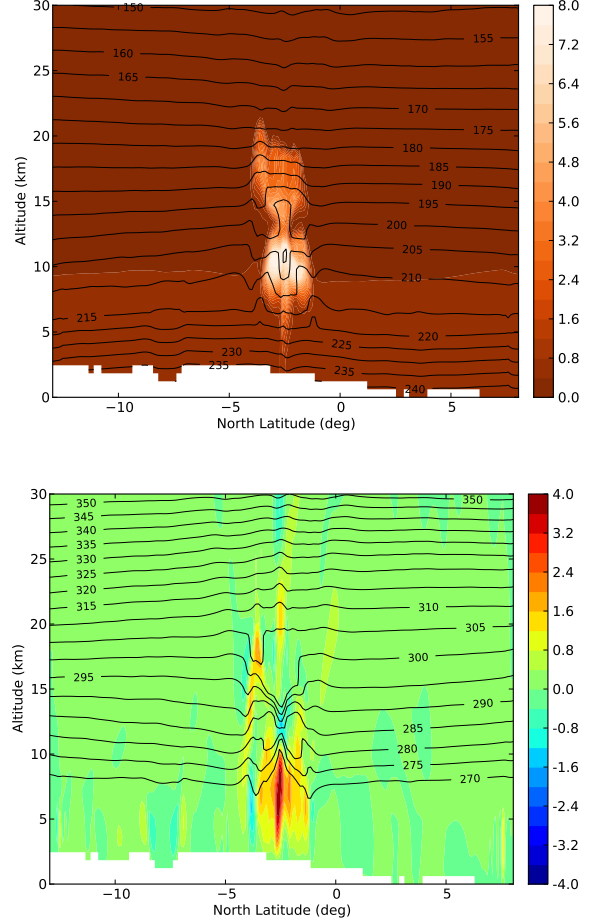


Figure 6: LMD-MMM reference simulation of the OMEGA storm. Latitude-altitude sections obtained at local time 15 : 00 and longitude 25°E. (top plot, shaded) MCS-like density-scaled optical depth in $10^{-3} \text{ m}^2 \text{ kg}^{-1}$. (top plot, contours) Temperature in K. (bottom plot, shaded) Vertical wind in m s^{-1} . (bottom plot, contours) Potential temperature in K.

where c_p is specific heat capacity, T temperature, t time, \mathcal{H} diabatic heating rate, $\mathcal{P} = (P/P_0)^{R/c_p}$ Exner function, R gas constant, P_0 reference pressure. This formulates how diabatic warming turns the dust disturbance into a warm bubble of potential temperature which subsequently rises. Here, $\mathcal{H} \simeq \mathcal{H}_{\text{SW}}$ and variations of \mathcal{H}_{SW} mostly follow variations of density-scaled optical depth (see Figure 5). Now, from the eulerian point of view, potential temperature θ at a given geometrical position in Figure 6 is modified both through diabatic processes \mathcal{J} and vertical advection of heat \mathcal{A}

$$\frac{\partial \theta}{\partial t} = \mathcal{J} + \mathcal{A} \quad \text{with} \quad \mathcal{A} = -w \frac{\partial \theta}{\partial z} \quad (10)$$

where w is vertical wind (horizontal transport of heat is neglected) and z altitude. At the top of the dust disturbance in Figure 6, potential temperature is larger than in the environment: \mathcal{J} is positive owing to radiative warming by dust particles while \mathcal{A} is close to zero because convective motions are not yet established. Conversely, at the bottom of the dust disturbance, potential temperature is lower than in the environment: \mathcal{A} is negative, since established vertical winds induce advection of air with lower θ from below, and overwhelms \mathcal{J} as dust particles (drivers for diabatic heating \mathcal{J}) are being transported upward. Hence the temperature and potential temperature disturbances in Figure 6 are governed by competing radiative warming and adiabatic cooling through ascent. Only fine-resolution mesoscale modeling is able to resolve this interplay between radiation and dynamics. We also note that emitted gravity waves impact temperature fields above the rocket dust storm.

In other words, rocket dust storms are radiatively-controlled dry convective storms. Similarly to terrestrial moist convection (see e.g. Holton, 2004), we shall define the Convective Available Potential Energy [CAPE] \mathcal{C} associated with Martian dust storms

$$\mathcal{C} = \int_{\text{storm}} g \frac{\Delta T}{T_{\text{env}}} dz \quad (11)$$

where T_{env} is the environmental temperature (outside the storm) and ΔT is the temperature contrast between inside and outside the storm disturbance (i.e.

the temperature of rising air parcels minus the environmental temperature). Assuming ideal energy transfer and negligible entrainment, the maximum vertical velocity w_{max} reached by convective updrafts writes

$$w_{\text{max}} = \sqrt{2\mathcal{C}} \quad (12)$$

A 5 km-deep dust plume undergoing, as in Figure 5, a radiative warming of $\Delta T \sim 7$ K during half an hour while its environment is at 250 K would rise vertically with typical velocity $w_{\text{max}} \sim 30 \text{ m s}^{-1}$ (corresponding CAPE is $\mathcal{C} \sim 500 \text{ J kg}^{-1}$). Clearly this theoretical calculation is an overestimate, in which significant entrainment and rapid plume rising are neglected, but the order of magnitude obtained from LMD-MMM simulations in Figure 5 is correctly accounted for. The meaning of this simple calculation is qualitative rather than quantitative: it illustrates that dust radiative effects have a strong potential to trigger deep convection on Mars.

Apart from large temperature contrast between inside and outside storm, rocket dust storms could reach high altitudes for two main reasons. Firstly, the upward transport of dust particles (and subsequent rising of the area where radiatively-induced warming is maximum) acts as a positive feedback for storm convective motions. Mesoscale simulations show that induced shortwave heating rates does not vary much when the OMEGA storm rises. Since environmental temperature decreases with altitude, this results in larger \mathcal{C} hence faster updrafts. Secondly, processes which could inhibit convection are not efficient. At pressures as low as 10 Pa, Stokes-Cunningham sedimentation velocities for dust micron-sized particles are still one to two orders of magnitude lower than convective velocity. Moreover, on Mars, no stable layer like the stratosphere on Earth is encountered by rising dust plumes whose summits are, as a consequence, less likely to resemble the “anvil” of terrestrial cumulonimbus. What really causes the rocket dust storm to stop rising is the abrupt drop in incoming sunlight at sunset.

Despite strong vertical acceleration, the OMEGA storm is still impacted by horizontal winds as is shown in Figure 4 (and movie in supplementary material). This is in line with MOC images in Figure 2.

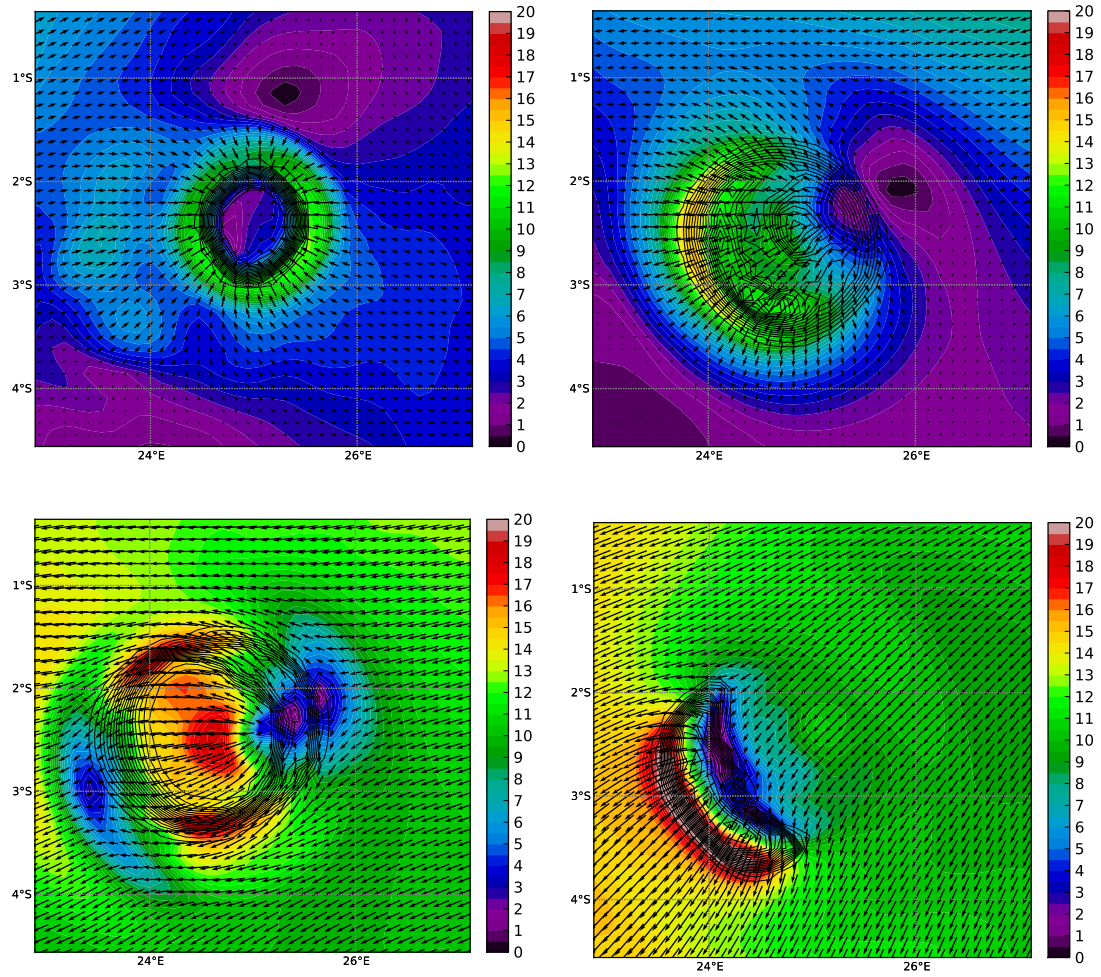


Figure 7: LMD-MMM reference simulation of the OMEGA storm. Maps of horizontal wind speed in m s^{-1} with wind vectors superimposed and density-scaled optical depth contoured. Top plots show local time 1400 and bottom plots local time 1500. Altitude above MOLA zero datum is 3 km (top left), 14 km (top right), 10 km (bottom left), 20 km (bottom right).

Tropospheric jet-streams act to gradually drift dust particles towards southwest, before the storm really loses its plume-like appearance after sunset and the sudden drop in convective energy supply. Mesoscale temperature gradients induced by the dust storm itself contribute to horizontal transport of dust particles. Hydrostatic equilibrium implies that those temperature gradients drive outward (inward) pressure forces at the summit (bottom) of the storm, therefore divergent (convergent) horizontal flow in the absence of significant Coriolis force. LMD-MMM predictions in Figure 7 show that horizontal inflow and outflow induced by rocket dust storms are significant and yield local modulations of large-scale winds by about a factor of 2. These thermally-induced horizontal motions cause a confinement of dust particles in the lower part of the storm and a dust storm widening near the summit.

Figure 8 displays the evolution of the dust cloud in the night and in the morning the following sol; maps of dust optical depth are omitted here because, from the nadir point of view, the high-altitude dust cloud is no longer discernible from background conditions. Figure 8 shows that dust particles initially composing the OMEGA storm in the afternoon form a clear-cut detached layer at nighttime. This detached layer of dust is predicted to occur at altitudes 25 – 30 km and to extend over large horizontal distances (more than 5° degrees longitude). It exhibits structure and altitude reminiscent of detached layers observed by MCS at pressure 10 – 100 Pa (Heavens et al., 2011a,b). Moreover, typical maximum values for density-scaled optical depth $\delta_z \tau_{\text{mcs}}$ in detached layers is predicted by LMD-MMM simulations to reach $\simeq 3$ to $6 \times 10^{-3} \text{ m}^2 \text{ kg}^{-1}$ in fair agreement with MCS observations of enriched layers of dust which range from 1 to $4 \times 10^{-3} \text{ m}^2 \text{ kg}^{-1}$ [cf. Figure 4 in Heavens et al. (2011a) and Figure 7 in Heavens et al. (2011b)]. Both MCS observations and mesoscale simulations indicate that density-scaled optical depth within high-altitude enriched layers of dust is about 2 to 10 times the value in lower troposphere. We thus show that dust storms in the lower troposphere, through their “rocket storm” behavior in the afternoon, have the ability to lead to detached layers of dust in the upper troposphere

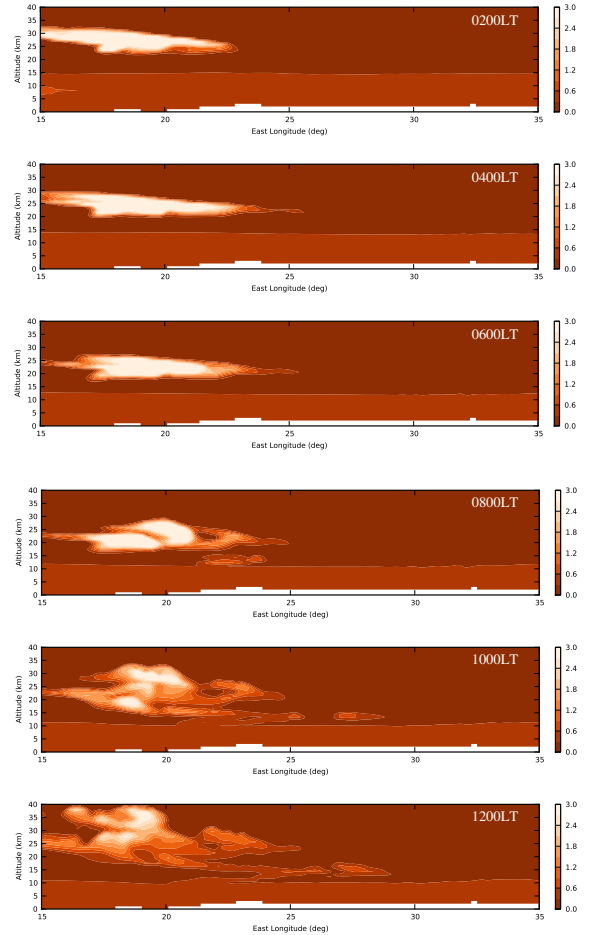


Figure 8: Same as Figure 4 except that section latitude is 4°S and local times 02 : 00 to 12 : 00 every two hours (from top to bottom).

within a few hours.

Furthermore, LMD-MMM simulations give insights into the lifetime of detached layers of dust. Figure 8 shows that the predicted high-altitude enrichment in dust particles in the morning is only slightly lower than in the previous evening. The most noticeable change of this dust cloud in six hours is instead a 5-km descent through sedimentation. This corresponds to downward vertical velocity of 0.2 m s^{-1} , consistent with the above-mentioned Stokes-Cunningham estimates. Enhanced radiative cooling yields a reversed thermal circulation in the dust cloud, which moderately reinforces downward motions in nighttime. This scenario for nighttime evolution could explain why dust detached layers are often located at higher altitude in daytime than in nighttime in MCS observations (Heavens et al., 2011a, though the authors recognize observational challenges might cast shadow on this conclusion).

There is a strong asymmetry between mesoscale processes leading to vertical transport of dust particles. Through convection, it only takes few hours for dust particles to rise from the lowermost troposphere to altitudes as high as 35 km; through sedimentation, it would take at least several sols for them to come back to their initial altitude. A detached layer of dust which persists in the Martian atmosphere the whole night is actually likely to stay until the following evening (provided no sudden increase in large-scale winds is encountered). Figure 8 shows indeed that, after sunrise, dust detached layers exhibit convective, plume-like, structures caused by the resupply of convective energy through absorption of visible sunlight by dust particles. This causes the dust detached layer in our case study to rise to altitudes 30 – 40 km. Through this mechanism, high-altitude enriched layers of dust are expected to survive for at least several sols, if not tens of sols, before changes in large-scale winds would cause density-scaled optical depth to drop as horizontal winds spread dust particles over large distances. There resides the potentially long lifetime of detached layers of dust in the Martian atmosphere.

4.2 Sensitivity simulations

Figure 9 summarizes the evolution of the OMEGA storm predicted by the LMD-MMM with reference settings: rocket dust storm in the afternoon, formation of a detached layer in the evening, descent through sedimentation in the night, ascent in the following morning which ensures detached layers are able to survive during several days. The robustness of this dynamical scenario is now confronted to additional simulations with modified settings.

4.2.1 Radiative forcing of storm disturbance

Absorption of incoming sunlight by dust particles is the supply of convective energy in rocket dust storms. A key sensitivity test is to assess the OMEGA storm evolution without the radiative effects of transported dust. To that purpose, we keep the column dust optical depth equal to TES column optical depth (i.e. background dust optical depth) in LMD-MMM radiative transfer calculations. Initial storm disturbance and LMD-MMM integrations are similar to the reference simulation. Dust particles in the storm perturbation are transported by atmospheric winds and undergo sedimentation, but play no radiative role.

From the nadir point of view, the storm lifetime is similar whether or not transported dust is radiatively active (in the two cases, column optical depth looks as in Figure 4). Storm lifetime is slightly longer in the radiatively-active case, owing to induced thermal circulations which imply convergence at the bottom of the storm and limit the horizontal spreading of dust particles by large-scale winds. Conversely, the limb point of view reveals major differences between the radiatively active and inactive cases (compare Figure 10 with Figure 4). Deep convective motions (rocket dust storm) and subsequent high-altitude enriched layers of dust are not predicted when transported dust is assumed to be radiatively inactive. In the absence of strong vertical winds, horizontal wind shear dominates the transport of dust particles. The initial dust disturbance is almost entirely dissipated in the end of the night under the influence of horizontal transport and sedimentation. Radiative effects of transported dust appear essential to initiate and

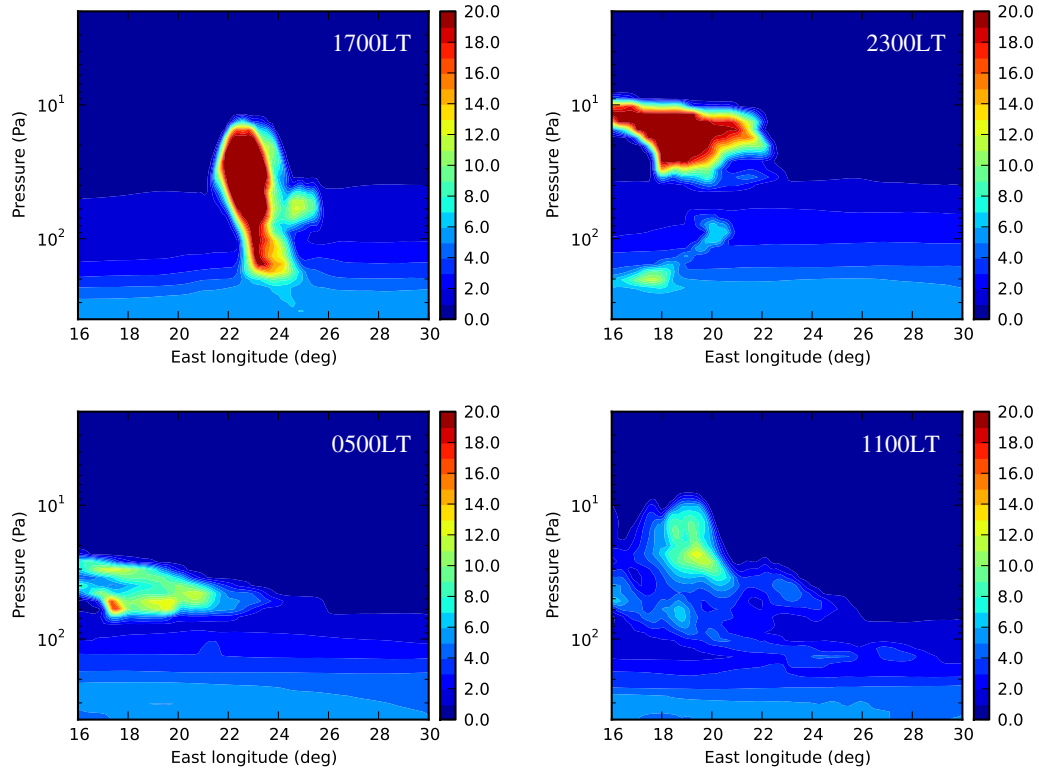


Figure 9: LMD-MMM reference simulation of the OMEGA storm. This figure provides a summary of the storm evolution: rocket dust storm in the afternoon (top left panel), formation of a detached layer in the evening (top right panel), descent through sedimentation in the night (bottom left panel), resuming ascent in the following morning which ensures detached layers are able to survive during several days (bottom right panel). Longitude-altitude sections of “MCS-like” density-scaled dust optical depth are shown as in Figures 4 and 8, except units are $10^{-4} \text{ m}^2 \text{ kg}^{-1}$ and results are averaged over latitudes ($0 - 5^\circ \text{S}$) so that the section latitude has not to be adapted to the southward drift of the OMEGA storm. The displayed local times are also distinct from Figure 4 and indicated on each panel.

maintain high-altitude detached layers of dust in the Martian atmosphere.

4.2.2 Properties of initial storm disturbance

Here we assess how sensitive the predicted evolution of the OMEGA storm is to assumptions made on the initial dust disturbance. The sensitivity simulations carried out to that purpose are listed in table 1. The reference case is case R. In cases n and nD, a more confined dust disturbance is considered to simulate the observed local maximum in dust optical depth in Figure 1. Case D is similar to case R except that the storm optical depth is larger. Case W explores the possibility that the OMEGA storm might actually be larger than the OMEGA footprint. Case LP is an alternative simulation designed to account for larger dust effective radius r_{eff} often observed in dust storms (see section 3.3). Case IT assumes an initial 5 km-high dust storm perturbation instead of the reference 10 km-high perturbation. Indeed, only transport and mixing below PBL top (~ 5 km in the considered location and season) can be undoubtedly assumed: assuming that the initial dust disturbance extends above the PBL top is implicitly assuming that deep convective mixing occurs (see section 4.1). Case E considers that the storm disturbance is not confined near the surface at the local time of OMEGA measurements (1330): as is suggested by both the analysis in section 4.1 and PFS measurements, the convective ascent of the storm has probably already started at that local time. Given the storm convective behavior, this scenario is equivalent to setting a disturbance similar to the reference case at an earlier local time (we chose 1130).

The results of sensitivity simulations are shown in Figure 11 for comparison with the reference case in Figure 9 (results for case D are close to case nD hence omitted). For all cases in Table 1, the storm evolution is qualitatively similar to the reference case: afternoon convection (rocket dust storm), evening detached layer, nighttime sedimentation, morning re-ascent which acts to maintain the detached layer. The reference simulation appears as typical of what could be obtained for a range of reasonable assumptions for the initial dust disturbance. A few elements

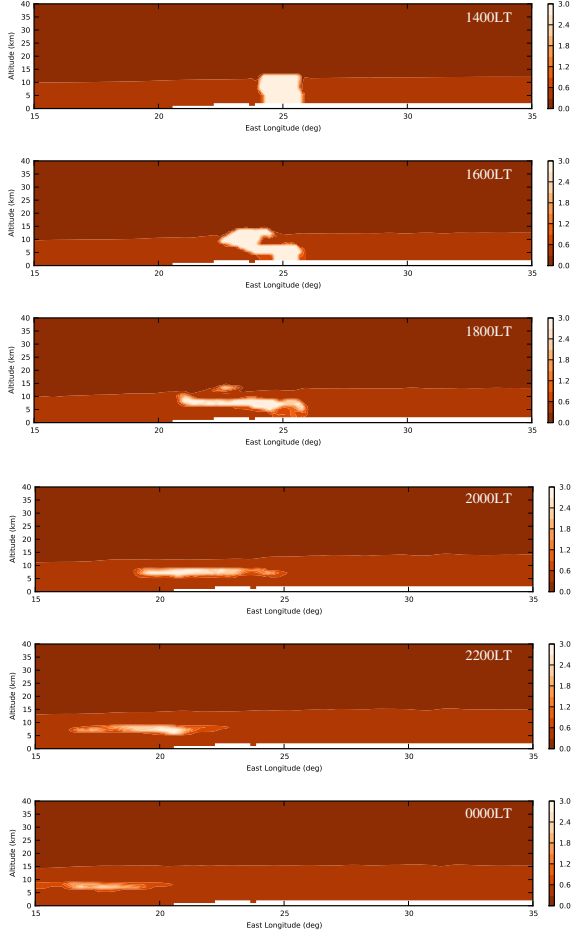


Figure 10: Same as Figure 4 except dust particles within storm are not radiatively active.

Case	Comments	τ_{storm}	R_{storm}	r_{eff}	Bottom-top altitudes
R	Reference	4.25	$0.5^\circ (\simeq 30 \text{ km})$	$1.5 \mu\text{m}$	0 – 10 km
n	Narrow	4.25	$0.1^\circ (\simeq 6 \text{ km})$	$1.5 \mu\text{m}$	0 – 10 km
nD	Narrow dustier	10	$0.1^\circ (\simeq 6 \text{ km})$	$1.5 \mu\text{m}$	0 – 10 km
D	Dustier	10	$0.5^\circ (\simeq 30 \text{ km})$	$1.5 \mu\text{m}$	0 – 10 km
W	Wide	4.25	$1.0^\circ (\simeq 60 \text{ km})$	$1.5 \mu\text{m}$	0 – 10 km
LP	Larger particles	4.25	$0.5^\circ (\simeq 30 \text{ km})$	$3.0 \mu\text{m}$	0 – 10 km
IT	Lower top	4.25	$0.5^\circ (\simeq 30 \text{ km})$	$1.5 \mu\text{m}$	0 – 5 km
E	Earlier storm	4.25	$0.5^\circ (\simeq 30 \text{ km})$	$1.5 \mu\text{m}$	0 – 10 km [1130LT]

Table 1: Parameters defining the initial dust disturbance and explored in the sensitivity study detailed in section 4.2 and Figure 11.

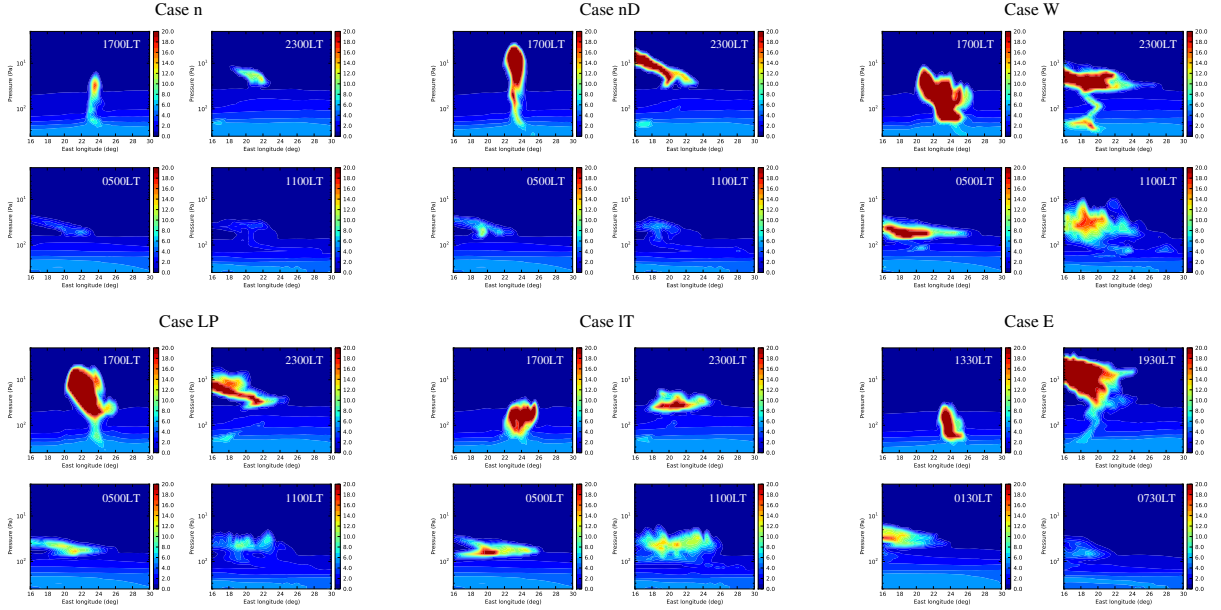


Figure 11: Figures analogous to Figure 9 for cases detailed in table 1 and described in section 4.2. Note that the displayed local times for case E are earlier than other cases (hence morning re-ascent is not shown contrary to other displayed cases). In cases n and nD (case W) lower (larger) values for dust-scaled optical depth compared to Figure 9 are caused by meridional averaging since storm radius is lower (larger). In cases LP and E, density-scaled optical depth in the morning dust cloud is less than in the reference simulation because the rocket dust storm reached higher altitudes characterized by enhanced horizontal winds which advect more dust particles out of the mesoscale domain.

in Figure 11 are worth being detailed.

- The size of initial perturbation does not impact the altitude reached by OMEGA dust storm by the end of the afternoon (cases nD and W). The main difference with the reference case R is the quantity of dust particles injected at high altitude (also worthy of notice in case W, 2 – 3 distinct rising plumes develop instead of one).
- A dustier storm injects particles at higher altitudes (cases D and nD). This is expected since radiative warming hence supply of convective energy are larger. The altitudes reached by dust storm particles in those cases (45 – 50 km) are probably overestimated though. Figure 1 indicates that the $\tau_{\text{storm}} = 10$ area is embedded into an area where optical depth is larger than assumed in cases nD and D where temperature contrast ΔT with the environment, and resulting CAPE, are therefore overestimated.
- The altitude of detached layers of dust in the night does not vary much with the initial dustiness of storm perturbation (compare e.g. cases n with nD). Dust particles reach higher altitudes in the end of the afternoon, but lower environmental densities cause larger sedimentation velocities in the night.
- The high-altitude enrichment of dust in the end of the afternoon is enhanced and occurs at higher altitudes if dust effective radius is assumed to be larger (case LP). Computation of dust radiative properties as in Madeleine et al. (2011) shows that larger r_{eff} yields slightly lower shortwave $Q_{\text{ext}}/r_{\text{eff}}$ ratio and larger longwave $Q_{\text{ext}}/r_{\text{eff}}$ ratio. Heating rates follow similar trends (equation 2). LMD-MMM simulations show indeed that increasing r_{eff} from $1.5 \mu\text{m}$ to $3 \mu\text{m}$ raises longwave heating rates from ~ 2 to ~ 8 K per Martian hour, while variations in shortwave heating rates are marginal (less than 10%). This yields enhanced CAPE \mathcal{C} within the rocket dust storm, hence enhanced vertical transport of dust particles. This is however mitigated in nighttime by enhanced sedimentation

rates associated with larger r_{eff} , as well as a more efficient thermally-induced circulation caused by enhanced longwave cooling. As a result, the altitude of dust detached layer in the end of the night is roughly similar to case R.

- The altitude reached by the rocket dust storm is 10 km lower for an initial perturbation more confined near the surface (case IT) than the reference case R. This apparently contradicts the larger supply of convective energy which stems from the larger density-scaled optical depths associated with near-surface confinement (predicted heating rates reach 30 K per Martian hour). Nevertheless, enhanced thermal circulations are associated with the warmer dusty disturbance, which causes reinforced divergence at storm top hence horizontal outflow of dust particles. As a consequence, the detached layer of dust in case IT forms at 20 – 25 km, at lower altitude than case R, but over larger latitudinal extent.
- When the storm simulation is started at local time 1130 (case E), the dust disturbance has risen to pressure ~ 100 Pa at local time 1330, in agreement with PFS measurements (cf. the approximate altitude of transition between negative and positive temperature anomalies in Figure 8 of Määttä et al. (2009)). Since the ascent of the rocket dust storm begins earlier than in the reference case, the maximum altitude reached is larger. Apart from this difference, the evolution of the dust detached layer in case E is similar to the reference case R.

4.2.3 Dust lifting

Our study focusses on the evolution of an observed, already established, dust storm perturbation. It is out of the scope of this paper to assess how the OMEGA storm initially appeared. Triggering a phenomenon such as the OMEGA dust storm probably requires a peculiar combination of large-scale and mesoscale processes. It is challenging to reproduce this with Martian mesoscale models which have not

yet reached the accuracy of their terrestrial counterparts. Furthermore, mechanisms governing the injection of Martian dust particles beyond the lowest couple of meters in PBL is still an open problem (cf. reviews by Greeley and Iversen, 1987; Kok et al., 2012).

Notwithstanding this, a less idealized case than those considered in sections 4.1 and 4.2 can be designed to assess both the birth and evolution of the OMEGA storm. The LMD-MMM is run in the same conditions as in the reference case, except no initial dust perturbation is assumed: instead dust lifting through near-surface winds is activated over the area covered initially by the OMEGA storm perturbation in the reference case. This allows us to simulate a more realistic evolution of the OMEGA storm (notably, possible feedbacks in which storm circulations impact dust lifting as in Rafkin, 2009) without addressing the complexity of storm initiation which requires dedicated studies.

A simple lifting scheme is adopted. The lifting of dust particles by near-surface winds is mainly a function of wind stress $\sigma = \rho u_*^2$ exerted on the surface. Friction velocity u_* can be approximately deduced from horizontal wind speed $u(z_1)$ predicted a few meters above the surface

$$u_* = \frac{k u(z_1)}{\ln(\frac{z_1}{z_0})} \quad (13)$$

where $k = 0.4$ is von Karman's constant and z_0 the roughness length (set to 1 cm in the LMD-MMM). To first order, the threshold stress $\sigma_t = \rho u_{*t}^2$ (with u_{*t} the threshold friction velocity) required to initiate particle motion depends on particle size. Models and wind tunnel experiments show that near-surface winds tend to catch large dust particles (10-100 μm) rather than micron-sized dust particles suspended in the Martian atmosphere (White, 1979; Newman et al., 2002). Thus saltation and sand-blasting are possibly playing a key role in dust lifting on Mars (Greeley, 2002). Hence the simplest estimate of σ_t for micron-sized particles is the value for large particles, which approximately ranges between 10 mN m^{-2} and 40 mN m^{-2} . Once this threshold is reached, the vertical flux of dust particles $\mathcal{V}_{\text{lift}}$ ($\text{kg m}^{-2} \text{s}^{-1}$) is estimated following White (1979) and Marticorena

and Bergametti (1995)

$$\mathcal{V}_{\text{lift}} = 2.61 \alpha \frac{\rho}{g} (u_* - u_{*t}) (u_* + u_{*t})^2 \quad (14)$$

where α is an efficiency coefficient in the range $[10^{-3}, 10^{-1}] \text{ m}^{-1}$. If $\sigma > \sigma_t$, dust mass mixing ratio q is modified in lowermost model layers given mixing coefficients and the vertical flux $\mathcal{V}_{\text{lift}}$ of dust particles lifted from the surface. The increase in number density N is obtained assuming lifted dust particles follow a lognormal distribution with effective radius 3 μm (see sections 3.3 and 4.2.2).

The values of lifting threshold σ_t and efficiency α appropriate for Mars are unknown and certainly not uniform over the planet. Yet the detection of the OMEGA storm hints at favorable lifting conditions (owing to either availability of dust at the surface or exceptional meteorological conditions). Hence low threshold is assumed: $\sigma_t = 5 \text{ mN m}^{-2}$. It is chosen so that $u_{*t} \sim 0.5 \text{ m s}^{-1}$, which ensures predicted peaks in near-surface winds imply lifting of dust particles from the surface (this optimistic value might not be so if hysteresis effects are at play, see Kok, 2010). We set $\alpha = 2 \times 10^{-3} \text{ m}^{-1}$ inside storm area (a typical value according to literature, Kahre et al., 2006; Rafkin, 2009) and $\alpha = 0$ outside. First-order calculations with equation 14 and chosen $[\alpha, \sigma_t]$ yield vertical flux $\mathcal{V}_{\text{lift}}$ compatible with dust mass mixing ratio q within storm calculated in section 3.3.

The LMD-MMM simulation is started in early afternoon as in the reference case. Dust lifting starts during the night under the influence of slope winds associated with cratered terrains. Contrary to daytime conditions, dust particles are confined near the surface in the night: ultra-stable conditions lead to shear-driven PBL mixing with limited vertical extent. This is analogous to the adverse influence of temperature inversion layers on the vertical transport of pollutants on Earth. Figure 12 shows that this results in a significant enrichment of dust in the lowermost PBL layers, the optical depth thereof reaching $\tau \sim 3$. Horizontal transport of dust is northward in early morning but turns southwestward towards the afternoon. During the morning, as the sun rises in the Martian sky, dust particles are being transported upward increasingly quickly as the near-surface dust distur-

bance turns into a rocket dust storm (Figure 12). Increasing incoming solar flux enhances the supply of convective energy through absorption by dust particles initially at low altitudes. Later in the afternoon, the resulting extinction of incoming sunlight passing through the top dust-rich layers does not prevent sufficient radiative warming to occur below. The day-time development of the rocket dust storm is also facilitated by the growth in PBL mixing depth up to about 5 – 6 km above the surface.

The convective behaviour of dust perturbations is associated with low-level convergence and enhancement of near-surface winds which in turn induce lifting of dust particles from the surface. This is reminiscent of the positive radiative-dynamical feedbacks described in Rafkin (2009), possibly giving rise in mid-latitudes to balanced circulations analogous to terrestrial hurricanes. In our mesoscale simulations, the feedback mechanism is however limited because the fast ascent of rocket dust storms yields low duration of storm-induced near-surface circulations capable to lift dust. A balanced low-level dust storm cannot establish in equatorial and tropical regions, as is also noted by Rafkin (2009). This is confirmed in our simulations by the absence of low-pressure cores in rocket dust storms. The short lifetime of the OMEGA storm is not caused by inefficient lifting (given our chosen threshold σ_t) but instead by the fast, convective, ascent of the dust disturbance.

Dust particles are being transported upward to altitudes 25 – 35 km within 2 – 4 hours to eventually form a dust detached layer. Figure 12 can be compared to Figure 4. The evolution of the storm disturbance is qualitatively similar to the reference case, except that the storm ascent seems to have already begun at local time 1330, which further justifies the sensitivity simulations carried out in section 4.2.2 (case E in Figure 11). Predictions in Figure 12 after a full simulated Martian sol (and similar predictions obtained in third simulated sol) also indicate that LMD-MMM results are not too sensitive to spin-up (i.e. the few hours at the beginning of a mesoscale simulation during which predictions adjust to GCM boundary conditions). All these elements tend to confirm the robustness of the storm evolution derived from the reference case, despite the

idealized character of its initial state.

5 Discussion

In the particular case of the OMEGA storm, LMD-MMM simulations demonstrate that local dust storms have the ability to form detached layer of dust through radiatively-induced convective motions, a behavior we proposed to name “rocket dust storm”. Physical mechanisms discussed for this particular case are general enough for similar rocket dust storms to appear in other regions and seasons. In this section, we discuss the expected spatial and seasonal variability of rocket dust storms, their impact on the vertical distribution of dust (notably the formation of detached layers of dust) and other consequences on the Martian dust cycle, thermal structure, atmospheric dynamics, cloud microphysics, chemistry, and robotic and human exploration.

5.1 Variability of rocket dust storms and subsequent detached layers of dust

Where and when are rocket dust storms expected to appear? For reasons detailed in section 4.2.3, we discuss other factors than the necessary condition of dust being available for lifting and lifting threshold being reached. For similar reasons, we consider here a given storm disturbance and do not discuss variability caused by the quantity of lifted dust particles initially composing the storm disturbance.

In rocket dust storms, convective energy is provided through absorption of incoming solar radiation by suspended dust particles. This makes solar energy input a crucial factor governing rocket dust storms: the further the dust disturbance from subsolar latitudes, the weaker the convection, the lower the altitude reached by transported dust particles.

A second key factor to control the strength of rocket dust storms is background dustiness. Convective motions would be particularly developed for large CAPE \mathcal{C} , which happens for large temperature contrasts ΔT between the storm and its environment. For a given input in solar energy, the less dusty the

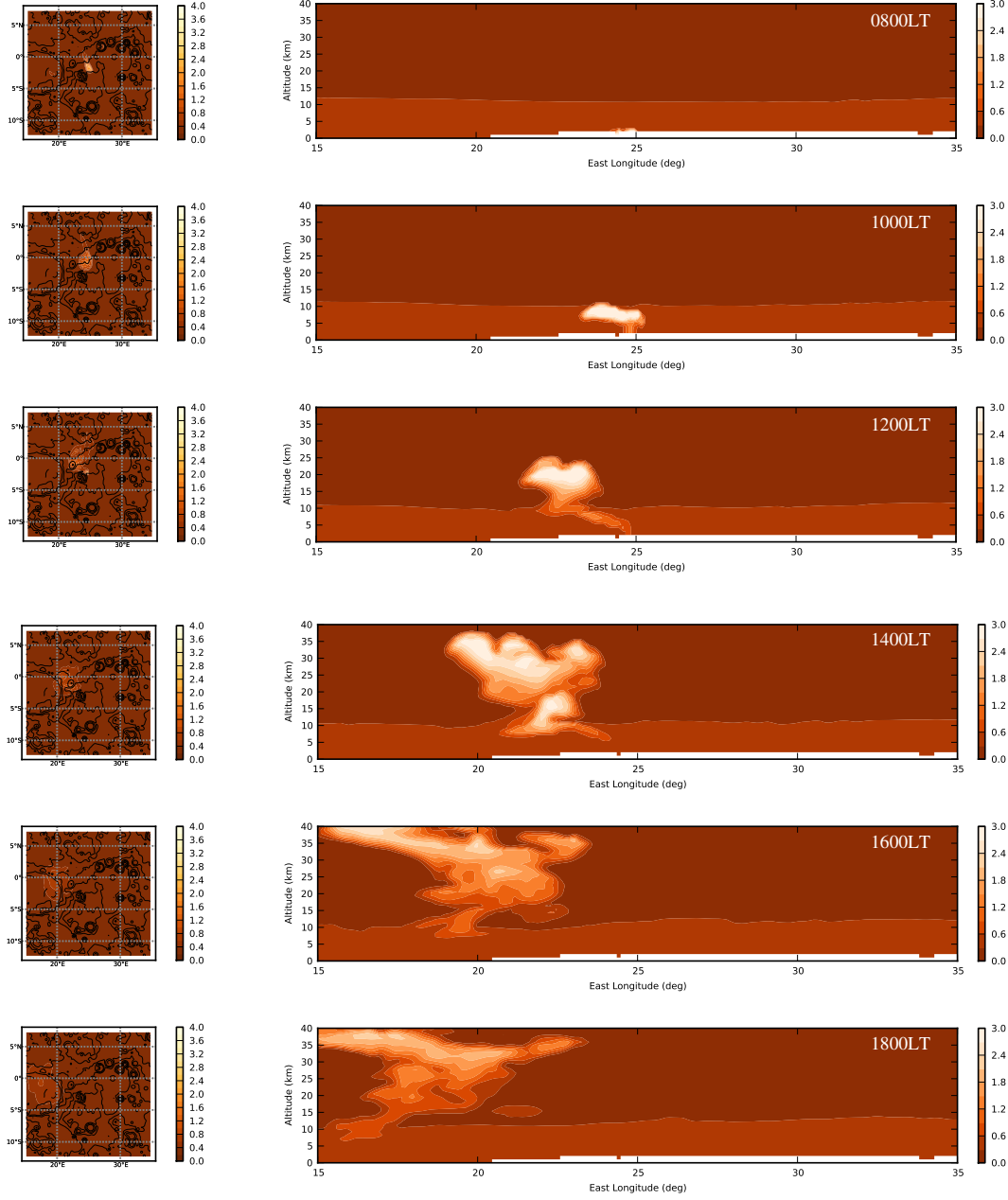


Figure 12: LMD-MMM storm simulation with lifting and no initial dust perturbation. Same as Figure 4 except that local times range from 0800 to 1800 and longitude-altitude sections are obtained at latitude 1.5°S.

background atmosphere, the lower the environmental temperature, the larger the vertical winds and altitudes reached by rocket dust storm. The OMEGA storm occurred at a season (late northern summer) when the Martian atmosphere is clear which, in addition to large incoming solar flux, explains why high altitudes are reached by this rocket dust storm. Conversely, we can simulate with the LMD-MMM what would have happened if the OMEGA storm had appeared in dusty northern winter, e.g. at $L_s = 240^\circ$. This solar longitude is chosen so that background dustiness is significantly increased compared to the reference case ($\tau_{\text{back}} = 0.6 - 0.7$ instead of $0.3 - 0.4$), while incoming solar energy is approximately similar. Results are shown in Figure 13. The dust disturbance does develop a convective behavior, but the warmer environment causes smaller values of CAPE C and vertical acceleration than in the reference case. Hence the rocket dust storm reaches lower altitudes ($15 - 20$ km) and loses its vertical extent earlier in the afternoon. The clearest seasons with respect to background dustiness appear more propitious to high-altitude rocket dust storms.

Two additional factors, while not as crucial as the two previous ones, could influence the development of rocket dust storms: atmospheric lapse rate and wind shear. Those are related to vertical variations of (respectively) temperature and horizontal winds. A more stable profile would tend to inhibit convective ascent of rocket dust storms. As the Martian atmosphere lacks a stratosphere, rocket dust storms are probably devoid of anvils at their summits that are common in terrestrial cumulonimbus. Yet contrasts in atmospheric stability could cause spatial and temporal variability in the altitude reached by rocket dust storms. This probably combines to the effect of background dustiness to make northern winter the least propitious season to high-altitude rocket dust storms (unless exceptionally dusty). Dustier background atmosphere implies warming in mid-troposphere and cooling in lower troposphere, hence a more stable temperature profile which would tend to mitigate vertical convective acceleration (as is the case in Figure 13). As far as horizontal wind shear is concerned, strong vertical shear could make rocket dust storms lose their ver-

tical extent, but this does not seem to happen when convective acceleration is significant. For instance, a strong near-surface vertical shear of horizontal wind does not prevent the OMEGA storm to develop and rise (see Figures 4 and 10).

We conclude that rocket dust storms would reach particularly high altitudes in tropical regions in northern spring and summer, where and when atmospheric dustiness is low. Detached layers of dust which result from the ascent and horizontal spreading of rocket dust storms, as is the case for the OMEGA storm (section 4), would tend to follow the same spatial and seasonal variability. In other words, if we assume that rocket dust storms are the source of detached layers of dust, we expect the latter to be particularly discernible in tropical regions in northern spring and summer. This is in agreement with the conclusions of Heavens et al. (2011a) based on MCS measurements about the presence of a so-called “high-altitude tropical dust maximum” throughout northern spring and summer. This maximum has a greater magnitude and altitude in the northern hemisphere. This can be easily understood since in spring/summer the northern hemisphere receives more incoming sunlight than the southern hemisphere, hence is more prone to strong rocket dust storms conducive to high-altitude detached layers. Furthermore, Heavens et al. (2011a) found in MCS measurements that the tropical dust maximum is particularly well-defined in the range $L_s = 110 - 160^\circ$ for MY28 and $L_s = 45 - 140^\circ$ for MY29, and related this difference to THEMIS and MARCI observations which showed a lack of “early season” tropical dust storm activity in MY28 compared to MY29. Finally, Heavens et al. (2011b) reported the significant longitudinal variability of the high-altitude tropical dust maximum, which maintained over time scales so large that dust lifting, transport and removal processes (i.e. fast mesoscale phenomena) must oppose advection, sedimentation and eddy diffusion (i.e. slow large-scale phenomena). This is in line with detached layers of dust being related to rocket dust storms.

Limb sounding by TES (Clancy et al., 2010, e.g. their Figure 10) and MCS (Heavens et al., 2011a, e.g. their Figure 5) show that northern winter (dusty season) is not devoid of detached layers of dust. The

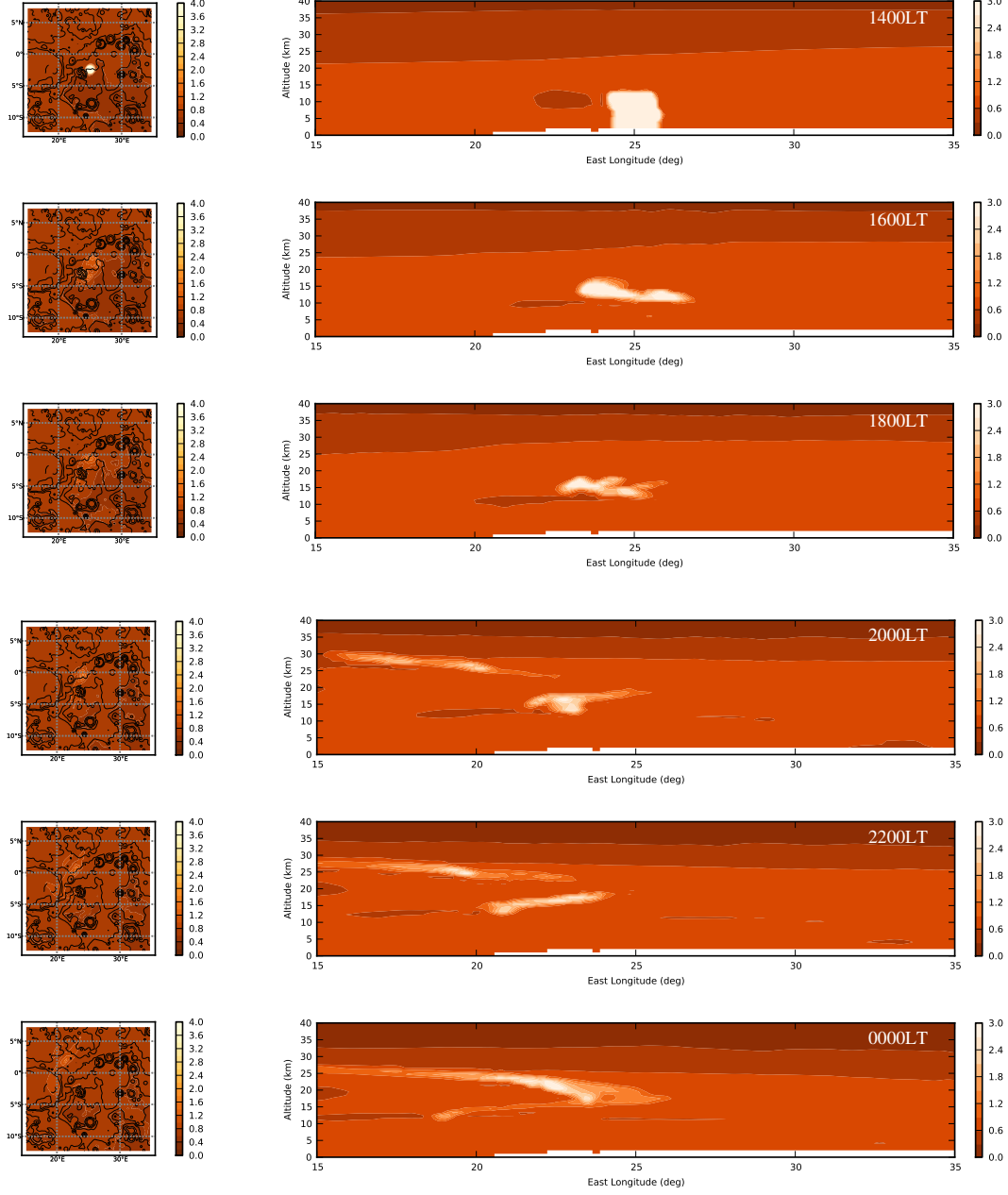


Figure 13: Same as Figure 4 except LMD-MMM simulation is performed at $L_s = 240^\circ$.

main distinction with northern spring/summer is how the altitude of enriched layers of dust compares with the summit of the background dust layer (roughly equivalent to what Heavens et al. (2011a) named falloff height). In northern spring/summer in tropical regions, the summit of the background dust layer is 40 km while it is 60 – 80 km in winter (e.g. Figure 4 and 5 in Montmessin et al., 2006). Hence enriched layers of dust are detected within the background dust layer in northern winter while they appear close to the summit of the background dust layer in spring/summer (if not above it). This seasonal contrast in the nature of detached layers is best summarized by Figure 1 in Heavens et al. (2011b). This difference can be related to the fact that background dustiness is larger in northern winter, which causes rocket dust storms to reach lower altitudes compared to northern spring/summer (Figure 13). In other words, rocket dust storms would tend to create enriched layers of dust within background dust layer in dusty season; and to form “truly detached” layers of dust in clear season, such as the high-altitude tropical dust maximum witnessed by MCS.

5.2 Sources of detached layers of dust

Not only rocket dust storms have the ability to form detached layers of dust at correct altitude and magnitude to first order (section 4.1), but could also account for their observed diurnal and seasonal variability, and to some extent their interannual and longitudinal contrasts (section 5.1). This posits that rocket dust storms are plausibly the best explanation for detached layers of dust in the Martian atmosphere.

One of the difficulties found by Heavens et al. (2011b) with this scenario is that MOC statistics of dust storm activity (Cantor et al., 2001, 2006) show that tropical dust storm activity is maybe too low to support the high-altitude tropical dust maximum. This difficulty is not irreconcilable with our conclusion that dust storms are a major source of detached layers of dust.

1. The limited horizontal extent and extremely fast evolution of rocket dust storms could prevent their detection by remote-sensing nadir

techniques with large footprints (THEMIS, TES) which can only monitor background dustiness and not mesoscale contrasts. We also found rocket dust storms possibly start their ascent in late morning instead of early afternoon (sections 4.2.2 and 4.2.3), which could prevent MGS/MOC, operating at local time 1400, from detecting most of those storms.

2. Not a large number of rocket dust storms are required for detached layers to be significantly loaded with dust particles. Our simulations show that a single rocket dust storm (constrained through observations) yields within a few hours a detached layer of dust which corresponds to typical values of density-scaled optical depth observed by MCS. Furthermore, we showed how detached layers of dust could survive for several sols once formed by rocket dust storms owing to slow sedimentation and daytime radiative warming of dust particles. Even intermittent rocket dust storms could lead to high-altitude detached layers of dust observable by MCS throughout northern spring/summer.
3. MOC statistics might be incomplete: tropical dust storms were observed in the tropics by Viking (cf. Figure 13 by Cantor et al., 2001); the OMEGA storm itself was detected in an area where dust activity is particularly low according to MOC, as is also the case for the convective-looking dust storm caught by the HiRISE camera in Figure 9 of Malin et al. (2008); dust optical depth measurements on board Mars Exploration Rovers in low latitudes exhibit sudden large variations in northern summer which are reminiscent of dust storm activity (Figure 13 in Smith et al., 2006).

Other potential sources for MCS detached layers of dust were explored by Heavens et al. (2011b). Mesoscale modeling by Rafkin et al. (2002) showed that anabatic (upslope) winds converging at the top of Arsia Mons lead to transport of dust particles at altitudes 20 km over large horizontal distances. While their contribution cannot be ruled out, Heavens et al. (2011b) noted that those cannot account for detached

layers of dust in areas distant from significant topography. A distinct scenario is that mesoscale circulations are not even involved in the formation of detached layers of dust: scavenging by water ice clouds could be a plausible explanation. Large water ice column optical depths, forming the aphelion cloud belt, are indeed observed when the high-altitude tropical dust maximum occurs (Wang and Ingersoll, 2002; Clancy et al., 2003). Heavens et al. (2011a) however resolved tropical maxima with MCS when the aphelion cloud belt is dissipated. We complement this statement by noting enriched layers within the dust background layer in northern winter (Clancy et al., 2010) cannot be accounted for by scavenging through water-ice clouds which are inexistent in the lower troposphere at this season. Heavens et al. (2011b) and Rafkin (2012) also argued that scavenging alone could not yield the observed high-altitude detached layers of dust with mixing ratios larger than in the lower troposphere. Significant mesoscale transport of dust particles is necessary for this to occur. Our mesoscale simulations of rocket dust storms are in line with those conclusions. Scavenging by water-ice clouds would only help to reinforce an existing detached layer of dust.

To explain the occurrence of high-altitude tropical dust maximum, Heavens et al. (2011b) also proposed to extend the idea of Fuerstenau (2006) that solar warming of suspended particles in dust devils could lead to convective acceleration and dust particles reaching altitudes as high as 15 – 20 km. This scenario suffers several possible limitations.

1. Compared to our computations for a $\tau \simeq 4$ storm, heating rates estimated by Fuerstenau (2006) within dust devils appear overestimated, especially given that dust devils are of lower optical depth than local dust storms and that large dust loading is mostly found at the edges of the vortex. In addition to this, THEMIS images in Towner (2009) indicate that dust devil cores are mostly colder than their environment.
2. While dust devils imply upward transport of large quantities of dust particles, an unrealistically large number of them would be necessary to advect as many dust particles as a rocket dust

storm extended over tens of kilometers such as e.g. the OMEGA storm (Figure 1).

3. Should dust devils be involved, regions propitious to their apparition (e.g. Amazonis Planitia, Fisher et al., 2005) would play a role in the spatial variability of detached layers of dust, which is not clearly observed.
4. Considering dust devils as individual convective towers as done in Fuerstenau (2006) and Heavens et al. (2011b) is not an entirely correct approximation. Dust devils form when dust get transported within convective vortices which arise as part of the complex turbulent growth of the unstable daytime PBL (Kanak et al., 2000). The adaptation of the simplified convection model of Gregory (2001) to Mars proposed by Heavens et al. (2011b) would actually be more applicable to rocket dust storms than to dust devils. This is acknowledged by the authors themselves, as well as the need to address questions related to dust devils through turbulent-resolving simulations that include radiatively-active transported dust particles.

5.3 Implications of dusty deep convection on Mars

Deep convection triggered by radiative effect of dust particles is a remarkable feature of the Martian meteorology with numerous implications.

Rocket dust storms, and their plausible intimate link with detached layers of dust, underline the importance of mesoscale phenomena in driving the dust cycle on Mars. This does not contradict but complements the role played by planetary-scale circulations in dust transport (Newman et al., 2002; Kahre et al., 2006; Madeleine et al., 2011). Our mesoscale simulations show indeed how detached layers of dust result from both rocket dust storms (for vertical transport) and large-scale horizontal winds (for horizontal spreading of dust particles). A notable consequence is that GCMs lack both temporal and spatial resolutions to simulate local storms, hence cannot accurately represent the vertical transport of dust

particles in the troposphere. Heavens et al. (2011a) noted that the observed dust distribution at northern summer, notably the high-altitude tropical dust maximum, cannot be reproduced by GCM simulations of Richardson and Wilson (2002) and Kahre et al. (2006), while agreement is better in northern winter. This can be understood as rocket dust storms are likely to be more active and reaching higher altitudes in the former than in the latter season (section 5.1). In a more general sense, quite similarly to moist convective cells in terrestrial climate, rocket dust storms could significantly contribute to vertical transport in the ascending branch of the Hadley cell (Rafkin, 2012).

The analogy with moist convective storms on Earth opens broader perspectives. We describe in section 4 how radiatively-induced deep convection in the Martian atmosphere significantly impacts wind and temperature fields. Rocket dust storms, as their terrestrial counterparts, are efficient ways to transport heat and momentum. We also show that detached layers of dust could be a significant source for atmospheric warming and supply of convective energy several sols after being formed by a rocket dust storm. Thus we expect rocket dust storms to have a strong impact on the Martian climate which will need to be taken into account in GCMs. This applies to

- thermal structure: Madeleine et al. (2011) noticed their GCM underestimates temperature at altitudes 20 – 40 km during rapid increases of column dust optical depth;
- predictability: Rogberg et al. (2010) showed how meteorological predictability error could grow large as a result of uncertainties in the dust distribution;
- atmospheric dynamics: vertical transport of heat and momentum in rocket dust storms could perturb thermal tides (Lewis and Read, 2003), trigger Rossby waves (especially within tropical latitudes, e.g. section 2 in Schneider and Liu, 2009) and couple to large-scale circulation to give rise to instabilities (e.g. the Madden-Julian Oscillation on Earth, Zhang, 2005).

A parameterization of mesoscale dust storms, similar to cumulus parameterization on Earth, appears necessary to improve GCM predictions on Mars.

The local impact of rocket dust storms is as important as their influence on the global climate. A potentially crucial element is the emission of mesoscale gravity waves by rocket dust storms. Gravity waves induce large temperature perturbations (Spiga et al., 2012) and, especially when they break, exert a drag on large-scale circulation which needs to be parameterized in Martian GCMs (Forget et al., 1999; Medvedev et al., 2011). By accounting for the convective source in addition to the (commonly considered) topographical one (Creasey et al., 2006), mesoscale simulations of rocket dust storms could help to improve both the interpretation of GW-induced phenomena, and GCM parameterizations. Mesoscale dynamical disturbances implied by rocket dust storms are actually crucial for the exploration of Mars in general. Figures 5 and 7 showed that large horizontal and vertical winds are associated with the occurrence of rocket dust storms. Modeled winds reach limits over which entry, descent and landing might not be safe (Vasavada et al., 2012). Thus the possibility that deep convection occurs in the Martian atmosphere shall be considered for designing and engineering future missions in the Martian environment. Rocket dust storms are all the more critical for the exploration of Mars as those could produce strong electric fields through triboelectric charging and give rise to lightning and radio emission (Renno et al., 2003; Ruf et al., 2009), as is the case for thunderstorms on Earth and other planetary atmospheres (Russell et al., 2011; Fischer et al., 2011).

Rocket dust storms do not only impact dust cycle and atmospheric circulation. Strong convective motions would induce fast upward transport of any molecule or aerosol present in the vicinity of the dust storm (before high-altitude jet streams induce extensive horizontal transport). A notable consequence for the Martian water cycle is that rocket dust storms could cause deep and efficient vertical transport of water vapor. This might help to explain the (often rapid) surge of detached layers of water vapor (Maltagliati et al., submitted to *Icarus*) and water ice clouds (Clancy et al., 2009; Vincendon et al., 2011) at

altitudes above 40 km. Possible upward transport of molecular species and aerosols by rocket dust storms has numerous implications too for photochemical cycles on Mars (Rafkin, 2012), especially if electrical activity is significant (Farrell et al., 2006). Rocket dust storms would also control the amount of condensation nuclei in the atmosphere, which is key to understand supersaturation on Mars (Maltagliati et al., 2011) and heterogeneous chemistry (Lefèvre et al., 2008).

The convective behavior evidenced here for local dust storms on Mars also apply to larger dust storms. Dust fronts, which develop at the edge of polar caps and as a result of baroclinic instability, sometimes exhibit convective-like appearance (Strausberg et al., 2005). Regional dust storms might be for rocket dust storms what mesoscale convective systems are for individual thunderstorms on Earth (Houze, 2004). A behavior similar to rocket dust storms, or a cluster thereof, might be involved in the development of Martian global dust storms, whose mechanisms are left to be explained. In addition to other factors such as the availability of dust reservoirs (Pankine and Ingersoll, 2002), the role played by mesoscale phenomena might explain why GCMs have difficulties reproducing the interannual variability of those events (Newman et al., 2002; Basu et al., 2006). This is a scientific problem probably worth being explored in the future with mesoscale models which, contrary to GCMs, have the ability to resolve convective motions.

References

- Anderson, E. and Leovy, C. (1978). Mariner 9 television limb observations of dust and ice hazes on Mars. *J. Atmos. Sci.*, 35:723–734.
- Balme, M. and Greeley, R. (2006). Dust devils on Earth and Mars. *Reviews of Geophysics*, 44:3003–+.
- Basu, S., Wilson, J., Richardson, M., and Ingersoll, A. (2006). Simulation of spontaneous and variable global dust storms with the GFDL Mars GCM. *Journal of Geophysical Research (Planets)*, 111(E10):9004.
- Cantor, B. A. (2007). MOC observations of the 2001 Mars planet-encircling dust storm. *Icarus*, 186:60–96.
- Cantor, B. A., James, P. B., Caplinger, M., and Wolff, M. J. (2001). Martian dust storms: 1999 Mars Orbiter Camera observations. *J. Geophys. Res.*, 106:23653–23688.
- Cantor, B. A., Kanak, K. M., and Edgett, K. S. (2006). Mars Orbiter Camera observations of Martian dust devils and their tracks (September 1997 to January 2006) and evaluation of theoretical vortex models. *Journal of Geophysical Research (Planets)*, 111(E10):12002–+.
- Clancy, R. T., Wolff, M. J., Cantor, B. A., Malin, M. C., and Michaels, T. I. (2009). Valles Marineris cloud trails. *Journal of Geophysical Research (Planets)*, 114(E13):11002.
- Clancy, R. T., Wolff, M. J., and Christensen, P. R. (2003). Mars aerosol studies with the MGS TES emission phase function observations: Optical depths, particle sizes, and ice cloud types versus latitude and solar longitude. *Journal of Geophysical Research (Planets)*, 108(E9):2–1.
- Clancy, R. T., Wolff, M. J., Whitney, B. A., Cantor, B. A., Smith, M. D., and McConnochie, T. H. (2010). Extension of atmospheric dust loading to high altitudes during the 2001 Mars dust storm: MGS TES limb observations. *Icarus*, 207:98–109.
- Conrath, B. J. (1975). Thermal structure of the Martian atmosphere during the dissipation of dust storm of 1971. *Icarus*, 24:36–46.
- Creasey, J. E., Forbes, J. M., and Hinson, D. P. (2006). Global and seasonal distribution of gravity wave activity in Mars’ lower atmosphere derived from MGS radio occultation data. *Geophys. Res. Lett.*, 33:1803.
- Elteto, A. and Toon, O. B. (2010). The effects and characteristics of atmospheric dust during martian global dust storm 2001A. *Icarus*, 210:589–611.

- Farrell, W. M., Delory, G. T., and Atreya, S. K. (2006). Martian dust storms as a possible sink of atmospheric methane. *Geophys. Res. Lett.*, 33:21203.
- Fischer, G., Kurth, W. S., Gurnett, D. A., Zarka, P., Dyudina, U. A., Ingersoll, A. P., Ewald, S. P., Porco, C. C., Wesley, A., Go, C., and Delcroix, M. (2011). A giant thunderstorm on Saturn. *Nature*, 475:75–77.
- Fisher, J. A., Richardson, M. I., Newman, C. E., Szewast, M. A., Graf, C., Basu, S., Ewald, S. P., Toigo, A. D., and Wilson, R. J. (2005). A survey of Martian dust devil activity using Mars Global Surveyor Mars Orbiter Camera images. *Journal of Geophysical Research (Planets)*, 110(E9):3004+.
- Forget, F., Hourdin, F., Fournier, R., Hourdin, C., Talagrand, O., Collins, M., Lewis, S. R., Read, P. L., and Huot., J.-P. (1999). Improved general circulation models of the Martian atmosphere from the surface to above 80 km. *J. Geophys. Res.*, 104:24,155–24,176.
- Fromm, M., Lindsey, D. T., Servranckx, R., Yue, G., Trickl, T., Sica, R., Doucet, P., and Godin-Beekmann, S. (2010). The Untold Story of Pyrocumulonimbus. *Bulletin of the American Meteorological Society*, 91:1193–1209.
- Fuerstenau, S. D. (2006). Solar heating of suspended particles and the dynamics of Martian dust devils. *Geophysical Research Letters*, 33:19.
- Gierasch, P. J. and Goody, R. M. (1972). The effect of dust on the temperature of the Martian atmosphere. *Journal of Atmospheric Sciences*, 29:400–402.
- Greeley, R. (2002). Saltation impact as a means for raising dust on Mars. *Planetary and Space Science*, 50:151–155.
- Greeley, R. and Iversen, J. (1987). *Wind as a Geological Process: On Earth, Mars, Venus and Titan*. Cambridge Univ Press.
- Gregory, D. (2001). Estimation of entrainment rate in simple models of convective clouds. *Quarterly Journal of the Royal Meteorological Society*, 127:53–72.
- Haberle, R. M., Leovy, C. B., and Pollack, J. B. (1982). Some effects of global dust storms on the atmospheric circulation of Mars. *Icarus*, 50:322–367.
- Heavens, N. G., Richardson, M. I., Kleinböhl, A., Kass, D. M., McCleese, D. J., Abdou, W., Benson, J. L., Schofield, J. T., Shirley, J. H., and Wolkenberg, P. M. (2011a). The vertical distribution of dust in the Martian atmosphere during northern spring and summer: Observations by the Mars Climate Sounder and analysis of zonal average vertical dust profiles. *Journal of Geophysical Research (Planets)*, 116(E15):4003.
- Heavens, N. G., Richardson, M. I., Kleinböhl, A., Kass, D. M., McCleese, D. J., Abdou, W., Benson, J. L., Schofield, J. T., Shirley, J. H., and Wolkenberg, P. M. (2011b). Vertical distribution of dust in the Martian atmosphere during northern spring and summer: High-altitude tropical dust maximum at northern summer solstice. *Journal of Geophysical Research (Planets)*, 116(E15):E01007.
- Holton, J. R. (2004). *An introduction to dynamic meteorology*, volume 48 of *International geophysics series*. Elsevier Academic Press, fourth edition.
- Houze, R. A. (2004). Mesoscale convective systems. *Reviews of Geophysics*, 42:4003.
- Jaquin, F., Gierasch, P., and Kahn, R. (1986). The vertical structure of limb hazes in the Martian atmosphere. *Icarus*, 68:442–461.
- Kahre, M. A., Murphy, J. R., and Haberle, R. M. (2006). Modeling the Martian dust cycle and surface dust reservoirs with the NASA Ames general circulation model. *Journal of Geophysical Research (Planets)*, 111(E10):6008.
- Kanak, K. M., Lilly, D. K., and Snow, J. T. (2000). The formation of vertical Vortices in the convective

- boundary layer. *Quarterly Journal of the Royal Meteorological Society*, 126:2789–2810.
- Kok, J. F. (2010). Difference in the Wind Speeds Required for Initiation versus Continuation of Sand Transport on Mars: Implications for Dunes and Dust Storms. *Physical Review Letters*, 104(7):074502.
- Kok, J. F., Parteli, E. J. R., Michaels, T. I., and Karam, D. B. (2012). The physics of wind-blown sand and dust. *ArXiv e-prints*.
- Lefèvre, F., Bertaux, J.-L., Clancy, R. T., Encrenaz, T., Fast, K., Forget, F., Lebonnois, S., Montmessin, F., and Perrier, S. (2008). Heterogeneous chemistry in the atmosphere of Mars. *Nature*, 454:971–975.
- Leovy, C. (1985). The general circulation of Mars : Model and observations. *Adv. Geophys*, 28a:327–346.
- Lewis, S. R. and Read, P. L. (2003). Equatorial jets in the dusty Martian atmosphere. *Journal of Geophysical Research (Planets)*, 108:5034–+.
- Määttänen, A., Fouchet, T., Forni, O., Melchiorri, R., Forget, F., Savijarvi, H., Bibring, J. P., Langevin, Y., Gondet, B., Formisano, V., and Giuranna, M. (2009). A study of the properties of a local dust storm with Mars Express OMEGA and PFS data. *Icarus*, 201(2):504–516.
- Madeleine, J.-B., Forget, F., Millour, E., Montabone, L., and Wolff, M. J. (2011). Revisiting the radiative impact of dust on Mars using the LMD Global Climate Model. *Journal of Geophysical Research (Planets)*, 116:11010.
- Malin, M. C., Calvin, W. M., Cantor, B. A., Clancy, R. T., Haberle, R. M., James, P. B., Thomas, P. C., Wolff, M. J., Bell, J. F., and Lee, S. W. (2008). Climate, weather, and north polar observations from the Mars Reconnaissance Orbiter Mars Color Imager. *Icarus*, 194:501–512.
- Maltagliati, L., Montmessin, F., Fedorova, A., Korabiev, O., Forget, F., and Bertaux, J.-L. (2011). Evidence of Water Vapor in Excess of Saturation in the Atmosphere of Mars. *Science*, 333:1868–.
- Martcorena, N. and Bergametti, G. (1995). Modeling the atmospheric dust cycle: design of a soil-derived emission scheme. *J. Geophys. Res.*, 102:16,415–16,430.
- McCleese, D. J., Heavens, N. G., Schofield, J. T., Abdou, W. A., Bandfield, J. L., Calcutt, S. B., Irwin, P. G. J., Kass, D. M., Kleinböhl, A., Lewis, S. R., Paige, D. A., Read, P. L., Richardson, M. I., Shirley, J. H., Taylor, F. W., Teanby, N., and Zurek, R. W. (2010). Structure and dynamics of the Martian lower and middle atmosphere as observed by the Mars Climate Sounder: Seasonal variations in zonal mean temperature, dust, and water ice aerosols. *J. Geophys. Res.*, 115(E14):12016–+.
- Medvedev, A. S., Yiğit, E., Hartogh, P., and Becker, E. (2011). Influence of gravity waves on the Martian atmosphere: General circulation modeling. *Journal of Geophysical Research (Planets)*, 116(E15):10004.
- Montabone, L., Lewis, S. R., and Read, P. L. (2005). Interannual variability of Martian dust storms in assimilation of several years of Mars global surveyor observations. *Advances in Space Research*, 36:2146–2155.
- Montmessin, F., Quémerais, E., Bertaux, J. L., Korabiev, O., Rannou, P., and Lebonnois, S. (2006). Stellar occultations at UV wavelengths by the SPICAM instrument: Retrieval and analysis of Martian haze profiles. *J. Geophys. Res.*, 111(E10):9.
- Murphy, J., Pollack, J. B., Haberle, R. M., Leovy, C. B., Toon, O. B., and Schaeffer, J. (1995). Three-dimensional numerical simulation of Martian global dust storms. *J. Geophys. Res.*, 100:26357–26376.
- Newman, C. E., Lewis, S. R., Read, P. L., and Forget, F. (2002). Modeling the Martian dust cycle 2. Multiannual radiatively active dust transport simulations. *Journal of Geophysical Research (Planets)*, 107:5124–+.

- Pankine, A. A. and Ingersoll, A. P. (2002). Inter-annual Variability of Martian Global Dust Storms. Simulations with a Low-Order Model of the General Circulation. *Icarus*, 155:299–323.
- Rafkin, S. C. R. (2009). A positive radiative-dynamic feedback mechanism for the maintenance and growth of Martian dust storms. *Journal of Geophysical Research (Planets)*, 114(E13):1009–+.
- Rafkin, S. C. R. (2012). The potential importance of non-local, deep transport on the energetics, momentum, chemistry, and aerosol distributions in the atmospheres of Earth, Mars, and Titan. *Planetary and Space Science*, 60:147–154.
- Rafkin, S. C. R., Sta. Maria, M. R. V., and Michaels, T. I. (2002). Simulation of the atmospheric thermal circulation of a martian volcano using a mesoscale numerical model. *Nature*, 419:697–699.
- Renno, N. O., Wong, A.-S., Atreya, S. K., de Pater, I., and Roos-Serote, M. (2003). Electrical discharges and broadband radio emission by Martian dust devils and dust storms. *Geophys. Res. Lett.*, 30(22):220000–1.
- Richardson, M. I. and Wilson, R. J. (2002). A topographically forced asymmetry in the martian circulation and climate. *Nature*, 416:298–301.
- Rogberg, P., Read, P. L., Lewis, S. R., and Montabone, L. (2010). Assessing atmospheric predictability on Mars using numerical weather prediction and data assimilation. *Quarterly Journal of the Royal Meteorological Society*, 136:1614–1635.
- Rossow, W. B. (1978). Cloud microphysics: Analysis of the clouds of Earth, Venus, Mars, and Jupiter. *Icarus*, 36:1,50.
- Ruf, C., Renno, N. O., Kok, J. F., Bandelier, E., Sander, M. J., Gross, S., Skjerve, L., and Cantor, B. (2009). Emission of non-thermal microwave radiation by a Martian dust storm. *Geophys. Res. Lett.*, 36:13202.
- Russell, C. T., Strangeway, R. J., Daniels, J. T. M., Zhang, T. L., and Wei, H. Y. (2011). Venus lightning: Comparison with terrestrial lightning. *Planet. Space Sci.*, 59:965–973.
- Schneider, T. and Liu, J. (2009). Formation of Jets and Equatorial Superrotation on Jupiter. *Journal of Atmospheric Sciences*, 66:579–+.
- Skamarock, W. C. and Klemp, J. B. (2008). A time-split nonhydrostatic atmospheric model for weather research and forecasting applications. *Journal of Computational Physics*, 227:3465–3485.
- Smith, M. D. (2004). Interannual variability in TES atmospheric observations of Mars during 1999–2003. *Icarus*, 167:148–165.
- Smith, M. D., Wolff, M. J., Spanovich, N., Ghosh, A., Banfield, D., Christensen, P. R., Landis, G. A., and Squyres, S. W. (2006). One Martian year of atmospheric observations using MER Mini-TES. *Journal of Geophysical Research (Planets)*, 111(E10):12–+.
- Spiga, A. and Forget, F. (2009). A new model to simulate the Martian mesoscale and microscale atmospheric circulation: Validation and first results. *Journal of Geophysical Research (Planets)*, 114:E02009.
- Spiga, A., Forget, F., Dolla, B., Vinatier, S., Melchiorri, R., Drossart, P., Gendrin, A., Bibring, J.-P., Langevin, Y., and Gondet, B. (2007). Remote sensing of surface pressure on Mars with the Mars Express/OMEGA spectrometer: 2. Meteorological maps. *Journal of Geophysical Research (Planets)*, 112(E11):8–+.
- Spiga, A., Forget, F., Lewis, S. R., and Hinson, D. P. (2010). Structure and dynamics of the convective boundary layer on mars as inferred from large-eddy simulations and remote-sensing measurements. *Quarterly Journal of the Royal Meteorological Society*, 136:414–428.
- Spiga, A., Forget, F., Madeleine, J., Montabone, L., Lewis, S. R., and Millour, E. (2011). The impact of Martian mesoscale winds on surface temperature and on the determination of thermal inertia. *Icarus*, 212:504–519.

- Spiga, A., González-Galindo, F., López-Valverde, M.-Á., and Forget, F. (2012). Gravity waves, cold pockets and CO₂ clouds in the Martian mesosphere. *Geophys. Res. Letters*, 39:2201.
- Spiga, A. and Lewis, S. R. (2010). Martian mesoscale and microscale wind variability of relevance for dust lifting. *International Journal of Mars Science and Exploration*, 5:146–158.
- Strausberg, M. J., Wang, H., Richardson, M. I., Ewald, S. P., and Toigo, A. D. (2005). Observations of the initiation and evolution of the 2001 Mars global dust storm. *Journal of Geophysical Research (Planets)*, 110(E9):2006.
- Szwast, M. A., Richardson, M. I., and Vasavada, A. R. (2006). Surface dust redistribution on Mars as observed by the Mars Global Surveyor and Viking orbiters. *Journal of Geophysical Research (Planets)*, 111(E10):11008.
- Thomas, P. and Gierasch, P. J. (1985). Dust devils on Mars. *Science*, 230:175–177.
- Toigo, A. D., Richardson, M. I., Wilson, R. J., Wang, H., and Ingersoll, A. P. (2002). A first look at dust lifting and dust storms near the south pole of Mars with a mesoscale model. *Journal of Geophysical Research (Planets)*, 107:5050–+.
- Towner, M. C. (2009). Characteristics of large Martian dust devils using Mars Odyssey Thermal Emission Imaging System visual and infrared images. *Journal of Geophysical Research (Planets)*, 114(E13):2010.
- Vasavada, A. R., Chen, A., Barnes, J. R., Burkhart, P. D., Cantor, B. A., Dwyer-Cianciolo, A. M., Ferguson, R. L., Hinson, D. P., Justh, H. L., Kass, D. M., Lewis, S. R., Mischna, M. A., Murphy, J. R., Rafkin, S. C. R., Tyler, D., and Withers, P. G. (2012). Assessment of Environments for Mars Science Laboratory Entry, Descent, and Surface Operations. *Space Science Reviews*, page 55.
- Vincendon, M., Pilorget, C., Gondet, B., Murchie, S., and Bibring, J. (2011). Observations of mesospheric CO₂ and H₂O clouds on mars. *Journal of Geophysical Research (Planets)*, 116:E00J02.
- Wang, H. and Ingersoll, A. P. (2002). Martian clouds observed by Mars Global Surveyor Mars Orbiter Camera. *J. Geophys. Res.*, 107:5078–+.
- Wang, H., Richardson, M. I., Wilson, R. J., Ingersoll, A. P., Toigo, A. D., and Zurek, R. W. (2003). Cyclones, tides, and the origin of a cross-equatorial dust storm on Mars. *Geophys. Res. Lett.*, 30:1488.
- White, B. R. (1979). Soil transport by winds on Mars. *J. Geophys. Res.*, 84:4643–4651.
- Wolff, M. J., Smith, M. D., Clancy, R. T., Arvidson, R., Kahre, M., Seelos, F., Murchie, S., and Savijärvi, H. (2009). Wavelength dependence of dust aerosol single scattering albedo as observed by the Compact Reconnaissance Imaging Spectrometer. *Journal of Geophysical Research (Planets)*, 114(E13):0–+.
- Zhang, C. (2005). Madden-julian oscillation. *Rev. Geophys.*, 43(2):1–36.
- Zurek, R. W. and Martin, L. J. (1993). Interannual variability of planet-encircling dust storms on Mars. *J. Geophys. Res.*, 98(E2):3247–3259.